Inner magnetosphere currents during the CIR/HSS storm on July 21–23, 2009

N. Y. Ganushkina,[1,2] S. Dubyagin,[1] M. Kubyshkina,[3] M. Liemohn,[2] and A. Runov[4]

Received 21 November 2011; revised 28 February 2012; accepted 29 February 2012; published 28 April 2012.

[1] Modeling results of the configuration of the inner magnetosphere current systems, namely, the ring current and the near-Earth tail current, during the July 21–23, 2009 CIR/HSS storm event are presented. We use two different modeling approaches, magnetic field modeling and particle modeling. We perform the magnetospheric magnetic field modeling with several standard and one modified Tsyganenko models, and the particle modeling with the Inner Magnetosphere Particle Transport and Acceleration Model (IMPTAM). It is found that the magnitudes of current densities in the inner magnetosphere computed with IMPTAM are comparable to those of computed with the TS05 magnetic field model. The model ring current, being asymmetric during the storm main phase did not show a duskward shift of its peak. It is shown with both modeling approaches that the incorporation of near-Earth tail currents in the calculations of model Dst (SymH in the present paper) index is crucial, as there is significant current beyond 6.6 R_E in the simulation results. A discrepancy is found between the SymH contributions from various currents as defined by the TS05 modules and from current streamline tracing through these same currents. We conclude that the method to calculate the contributions of different current systems to the model Dst using the global magnetospheric magnetic field models should be Biot-Savart integration inside the regions, which contain the current systems, not using the magnetic field from the model representations of current modules.

Citation: Ganushkina, N. Y., S. Dubyagin, M. Kubyshkina, M. Liemohn, and A. Runov (2012), Inner magnetosphere currents during the CIR/HSS storm on July 21–23, 2009, *J. Geophys. Res.*, *117*, A00L04, doi:10.1029/2011JA017393.

1. Introduction

[2] Two main current systems in the inner magnetosphere are the ring current (including its eastward, symmetric and partial components) and the near-Earth tail current. They flow across the magnetic field and distort the inner magnetosphere from its typical quiet time configuration [*Parker and Stewart*, 1967; *Tsyganenko et al.*, 2003; *Ganushkina et al.*, 2004]. The interpretation of currents in the inner magnetosphere is important for understanding the physics governing particle flow but it is difficult. Investigation of the relative locations, intensities, and variability of near-Earth currents is crucial to understanding the geospace dynamics.

[3] It is problematic to obtain near-Earth currents from observations. Currents can be calculated directly from magnetometer measurements, for example, from four closely located space satellites, such as the Cluster mission [e.g., *Vallat et al.*, 2005]. Currents (or their related magnetic perturbations) can be compiled statistically from all available data, and then binned according to some relevant parameter [e.g., *Zanetti et al.*, 1984; *Tsyganenko*, 1989, 1995; *Lui et al.*, 1994; Lui, 2003; *Le et al.*, 2004]. It is possible to determine local current intensities from observed plasma pressure time series [e.g., *Lui et al.*, 1987]. Magnetospheric currents have even been extracted from inversions of energetic neutral atom (ENA) images [*Roelof et al.*, 2004].

[4] When studying the global distribution of currents and their time variations during storms, there are usually not enough data available. One way of dealing with it is to use magnetic field models which can help to address the question regarding which of the current systems is responsible for what effects in the inner magnetospheric field distortion during storms. Several studies have been devoted to the development of general-purpose, global empirical magnetic field models [e.g., *Tsyganenko*, 1995, 2002a, 2002b; *Tsyganenko and Sitnov*, 2005, 2007; *Hilmer and Voigt*, 1995; *Alexeev et al.*, 2001]. A time-evolving empirical model called the event-oriented model [*Ganushkina et al.*, 2002, 2004] uses in-situ observations of the magnetospheric magnetic field for a specific storm event and

[1]Finnish Meteorological Institute, Helsinki, Finland.
[2]Department of Atmospheric, Oceanic, and Space Sciences, University of Michigan, Ann Arbor, Michigan, USA.
[3]Institute of Physics, St. Petersburg State University, St. Petersburg, Russia.
[4]Institute of Geophysics and Planetary Physics, University of California, Los Angeles, California, USA.

0148-0227/12/2011JA017393

adjusts a statistical solution to give a global representation of the magnetic field evolution for that specific storm event.

[5] Another way to obtain the magnetic field in the magnetosphere is from MHD modeling. The proper representation of the inner magnetosphere in global MHD by coupling with inner magnetosphere/ring current/radiation belt models is an important, but still open issue, which is under intense investigation at present. In their recent study, *Liemohn et al.* [2011] have used the Space Weather Modeling Framework (SWMF) for the numerical simulations. They have argued that a single near-tail magnetic field line can be part of a variety of cross-field current systems. One of the important implications was that magnetospheric current systems do not map well to characteristic features of the particle populations.

[6] The third approach for studying the currents in the inner magnetosphere, mainly, the ring current, is particle modeling. There exist several models for the ring current. The most extensively used are the modifications of RAM (Ring current Atmosphere interactions Model) developed initially by *Fok et al.* [1993] and *Jordanova et al.* [1996]. There are several variations of this model currently in use for the magnetospheric physics studies [e.g., *Fok et al.*, 2003; *Jordanova et al.*, 2006; *Khazanov et al.*, 2004; *Zheng et al.*, 2006; *Liemohn et al.*, 2006]. These models solve the gyration and bounce averaged kinetic equation for the main hot particle species (H^+, O^+, He^+, and electrons) in the keV energy range. There are three more models [*Chen et al.*, 1993; *Ebihara and Ejiri*, 2000; *Ganushkina et al.*, 2005], where the particle motion is followed in the drift approximation, and the Liouville theorem is used for particle flux calculations. Most of the models include Coulomb collisional scattering and decay, precipitation loss to the upper atmosphere, and charge exchange loss. Another widely used inner magnetosphere model is the Rice Convection Model (RCM), which describes plasma electrodynamics in the inner and middle magnetosphere and its coupling to the ionosphere [*Wolf et al.*, 1982; *Spiro et al.*, 1981]. The recently developed Rice Convection Model Equilibrium (RCM-E) [*Toffoletto et al.*, 2003; *Lemon et al.*, 2003] combines the drift physics and magnetosphere-ionosphere coupling computational machinery of the RCM with a model of equilibrium magnetic field in static force balance with the RCM-computed pressures.

[7] Studies of the contributions to the Dst index from different current systems have come to quite different conclusions. For example, *Liemohn et al.* [2001] examined the currents from a near-Earth hot ion drift physics model, concluding that most (at times nearly all) of the main phase Dst perturbation was from the partial ring current. *Søraas et al.* [2002] investigated specifically whether the depressed pressure corrected Dst-index during geomagnetic storms could be due to other current systems than the ring current. They compared a calculated Ring Current index (RC-index) based on the night side isotropic proton precipitation with the Dst-index and found that the two indices correlated well. At the same time, the role of the magnetotail current as a major contributor to the storm-time Dst perturbation was emphasized [*Alexeev et al.*, 1996; *Dremukhina et al.*, 1999; *Turner et al.*, 2000]. It was shown that the relative contributions of the ring current and tail current to Dst change during the course of storms [*Ganushkina et al.*, 2004, 2010; *Kalegaev et al.*, 2005]. *Ohtani et al.* [2006, 2007] found that for a given value of SymH, the ENA emission from the ring current is more intense and the geosynchronous magnetic field is more stretched during the main phase than during the recovery phase and suggested that the relative contribution of the ring current (tail current) is more significant during the main phase (recovery phase). *Ganushkina et al.* [2004] found that the Dst index for moderate storms (Dst > −150 nT) is dominated by the tail current and for more intense storms (Dst < −150 nT) is dominated by the ring current. The relative contribution also changes during the course of storm-time substorms [*Ohtani et al.*, 2001; *Pulkkinen et al.*, 2006; *Kubyshkina et al.*, 2008].

[8] It is well-known that the geomagnetic storms are very important phenomena for magnetospheric physics and for space weather. They have their origin in the structure and dynamics of the Sun. One type of the storms are driven by interplanetary coronal mass ejections (CMEs) associated with large eruptions of plasma and magnetic flux from the Sun [*Gosling et al.*, 1991; *Tsurutani and Gonzalez*, 1997]. The other type of the storms are driven by high speed streams (HSS) from coronal holes and the corotating interaction region (CIR) formed ahead of the stream [*Burlaga and Lepping*, 1977; *Gonzalez et al.*, 1999]. *Borovsky and Denton* [2006] have formulated the features of a HSS/CIR storm: (1) The interplanetary (IP) medium shows a stream interaction, where a fast stream (speed 700 km/s) overtakes a slower stream (speed 400 km/s); (2) The HSS interface is marked by a time moment, ahead of which the solar wind proton density and interplanetary magnetic field (IMF) are enhanced; (3) Interplanetary electric field is highly fluctuating but remains enhanced above 2 mV/m in the vicinity of, and following the stream interface; (4) The 3 hour averaged Kp index reaches a maximum a few hours before the Dst minimum; (5) The high density plasma in the low velocity stream and the simultaneous IMF B_z decrease cause the initial phase of the magnetic storm; (6) During passage of the interaction region the driving of the magnetosphere is mainly through the large negative IMF B_z excursions, reaching peak values right at the leading edge of the HSS; (7) In the high-speed flow behind the interaction region, the north-south component B_z is highly fluctuating, causing significant Dst and Kp activity for several days. These storms are the dominant sources of geomagnetic activity in the solar cycle declining phase [*Tsurutani et al.*, 2006]. Their magnitude is usually small, with average Dst of −50 nT [*Richardson et al.*, 2006; *Søraas et al.*, 2004]. *Denton et al.* [2006] and *Borovsky and Denton* [2006] concludes that the weaker ring current in CIR events is due to a less dense plasma sheet and a weaker convection field compared to what is observed during CME storms. However, HSS/CIR storms are effective in enhancing the electron fluxes in the outer radiation belt [*Miyoshi and Kataoka*, 2008].

[9] Several studies were devoted to the investigation of the behavior of current systems especially during CIR/HSS storms. Both observational and magnetic field and particle modeling approaches were used. *Jordanova et al.* [2009] have studied the ring current dynamics during the HSS-storm with RAM code [*Jordanova et al.*, 1996]. Their simulations were unsuccessful to reproduce the observed Dst-index. They found that radial diffusion and substorm injections are needed in order to reproduce the long-lasting

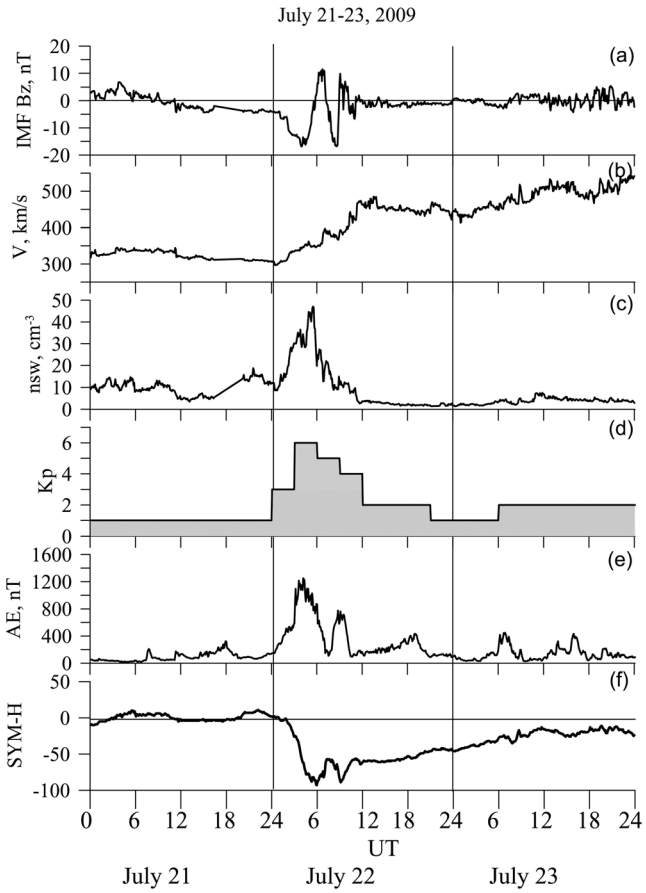

Figure 1. Overview of July 21–23, 2009 magnetic storm (see text).

recovery phase of HSS-driven storms. *Borovsky and Denton* [2010] have performed a superposed epoch analysis on the magnetic field measurements from five geosynchronous GOES spacecraft during HSS-driven storms to study the stretching of the nightside magnetosphere. They estimated that this nightside strong stretching perturbation contributes about 25% to the pressure-corrected Dst. *Sørbø et al.* [2009] investigated properties of the ring current during CIR/HSS events by the dynamics of the equatorward boundary of isotropic proton precipitation. They found that the injection of fresh particles balance the loss of ring current energy and the long recovery of the CIR/HSS events were reproduced by the RC-index computed using isotropic boundaries. *Sitnov et al.* [2010] have presented the empirical reconstruction of the magnetospheric magnetic field configuration for one CIR-driven storm. It was found that, compared to CME-driven storms, the model equatorial currents are more dawn dusk symmetric. Moreover, a new tail-type currents are found to dominate the storm-time magnetosphere in the early main and recovery phases at the moments of strong peaks of the solar wind dynamic pressure.

[10] The present paper contains the modeling results of the configuration of currents during the July 21–23, 2009 CIR/HSS storm event. We focus on the inner magnetosphere current systems, namely, the ring current and the near-Earth tail current. We use two different modeling approaches, magnetic field modeling and particle modeling. We do the magnetic field modeling with Tsyganenko models, such as T96 [*Tsyganenko*, 1995], T02 [*Tsyganenko*, 2002a, 2002b] and TS05 [*Tsyganenko and Sitnov*, 2005] and its modification, and particle modeling with the Inner Magnetosphere Particle Transport and Acceleration Model (IMPTAM), developed by *Ganushkina et al.* [2001, 2005, 2006, 2011]. We analyze similar outputs from two approaches, the evolution of current densities in the inner magnetosphere during CIR/HSS storm and contributions of the tail and ring currents to the Dst (or SymH in our case) index. The importance of the choice of the method for the model Dst calculations, both for magnetic field and particle modeling, is emphasized. The model Dst-contributions directly depend on the method. This study contributes to the still unresolved problem of the interpretation of currents in the near-Earth magnetotail and inner magnetosphere.

2. July 21–23, 2009 Storm Event Overview

[11] The magnetic storm on July 21–23, 2009 (Figure 1) occurred at the very beginning of the rising phase of solar cycle 24. Solar cycle 23 had a deep minimum and the Sun was very quiet and there was not much geomagnetic activity. A smooth southward turning of the IMF B_z (Figure 1a), which started around 11 UT on July 21st, caused a rather small storm. IMF B_z reached −17 nT at 0330 UT on July 22nd, oscillated couple of times between +10 nT and −17 nT and then from 12 UT was very close to zero till the end of the storm. A high-speed stream reached the Earth with a speed of about 500 km/s at 12 UT on July 22nd (Figure 1b). The HSS interface is marked by a time moment, ahead of which the solar wind proton density is enhanced. The peak of 46 cm^{-3} is seen in solar wind number density around 06 UT on July 22nd (Figure 1c). The magnetosphere responded with Kp = 6 around 6 UT on July 22nd (Figure 1d), and substorm activity with two main peaks in AL-index, one of 1200 nT at 04 UT and the other of 700 nT at 09 UT (Figure 1e). The SymH index dropped to about −90 nT at 06 UT and then to about −86 nT around 09 UT (Figure 1f). The solar wind and IMF parameters have been shifted to the Earth's subsolar point by OmniWeb (http://omniweb.gsfc.nasa.gov/form/omni_min.html). The activity indices were obtained from the World Data Center for Geomagnetism, Kyoto (http://wdc.kugi.kyoto-u.ac.jp/).

3. Modeling Approaches

3.1. Models for Magnetospheric Magnetic Field

3.1.1. Tsyganenko Magnetic Field Models

[12] For our modeling we use three different Tsyganenko magnetospheric magnetic field models, specifically T96 [*Tsyganenko*, 1995], T02 [*Tsyganenko*, 2002a, 2002b] and TS05 [*Tsyganenko and Sitnov*, 2005].

[13] The T96 model [*Tsyganenko*, 1995] was a step forward from only Kp-dependent previous versions [*Tsyganenko*, 1989]. It has several essential features such as (1) parameterization by the Dst-index, solar wind dynamic pressure, and B_y and B_z components of the interplanetary magnetic field (IMF), (2) a realistic shape and size of the magnetopause controlled by the solar wind, (3) controlled shielding of the magnetic field produced by all magnetospheric current systems, (4) the interconnection of the geomagnetic field with the IMF across

the magnetopause which can produce open magnetospheric configurations, and (5) the magnetic field of the Region 1 and 2 Birkeland currents. At the same time, its main problems included (1) overstretched magnetic field in the inner magnetosphere, and (2) absence of dawn-dusk asymmetry of the inner magnetosphere during storm periods. For the development of this model, the data sets in which storm-time observations were mixed with quiet time data were used.

[14] To include not only the current state of the interplanetary medium but also its time history during the preceding 1hour interval, another model was developed. In this T02 model [*Tsyganenko*, 2002a, 2002b], in addition to parametrization by Dst-index, solar wind dynamic pressure, and B_y and B_z components of the IMF, the strengths of all current systems at any given time included terms with the factors G1 and G2, defined as integrals of geoeffective IMF-related parameters over the preceding 1-hour interval. Improved representations were introduced for all major current systems, such as (1) axisymmetric and partial components of the model ring current, originally derived from charged particle data, (2) a flexible global model of the contributions of large-scale Region 1 and 2 Birkeland currents, and (3) a cross-tail current sheet representation with two modules with different rates of current density variation along the tail axis, a movable inner edge, variable thickness, and flexible shape, controlled by the tilt angle of the Earth's dipole. Although this model is more suitable for storms, it is valid only inside 15 R_E and does not include substorm variations of the magnetic field.

[15] A later version TS05 [*Tsyganenko and Sitnov*, 2005] has a similar mathematical structure but the data used were only for 37 storms with Dst < −65 nT that occurred between October 1996 and November 2000 [*Tsyganenko et al.*, 2003]. A new element was the way of parameterizing the model, in which each source of the magnetic field would have its own relaxation timescale and a driving function, based on an individual best fit combination of the solar wind and IMF parameters. The model parameters include the Dst-index, solar wind dynamic pressure, B_y and B_z components of the IMF, and six variables W_i, $i = 1, 6$. These variables W enter in the six magnitude coefficients for the magnetic fields from each source. Unlike T02, tail current thickness varies depending on the tail current driving parameter. This model has similar limitations as T02, such as (1) it is valid only inside 15 R_E and (2) does not include substorm variations of the magnetic field. A serious flaw of these models stems from their modular structure. The different modules can occupy the same space and sometimes produce not-physical configurations (e.g. thin tail current piercing thick ring current region).

[16] We use solar wind and IMF parameters and the Dst index as inputs for these models and calculate other model parameters as combinations of them (such as G parameters for the T02 model) and use pre-computed yearly input data files provided at the Tsyganenko models' web page (http://geo.phys.spbu.ru/~tsyganenko/TS05_data_and_stuff).

3.1.2. Adaptive Modeling for Magnetospheric Magnetic Field

[17] A way to improve a standard statistical model is to adjust its input parameters to best describe the observations available for the modeled period [*Kubyshkina et al.*, 2009]. This type of calculations is called adaptive modeling for the magnetospheric magnetic field. In previous studies, the event-oriented approach has been used [*Kubyshkina et al.*, 1999; *Ganushkina et al.*, 2004, 2010], in which the standard Tsyganenko model was modified by scaling the existing current systems and introducing additional ones. The free parameters for each current system were determined and then varied to find the set of the parameters that gives the best fit between the model and all available in-situ magnetic field observations. This modeling was used to obtain a realistic magnetic field configuration for specific events [*Ganushkina et al.*, 2004; *Kalegaev et al.*, 2005].

[18] Although this approach allows one to incorporate different observations for comparisons (e.g., magnetic field, plasma pressure, low-altitude measurements), we have chosen the simplest one. Specifically, magnetic field spacecraft observations and 5-minutes averaged SymH index were used to estimate model quality. The SymH index was treated here as one more spacecraft. After experimenting with different base models (T96, T02, TS05), we ended up with the modification of the TS05 model. In the modified TS05m model, two variable multipliers to TS05 current systems were introduced. The first (*amt*1) is the multiplier to the amplitude of the tail (short) module. The second (*amr*) is the multiplier to the ring current module amplitudes. The same multiplier was used for both symmetric and partial ring current modules. This method keeps a constant relation of contributions of the partial and symmetric ring current modules. Using the notations of *Tsyganenko and Sitnov* [2005], the total field of the magnetospheric sources $\mathbf{B}^{(mod)}$ has the form

$$\begin{aligned}\mathbf{B}^{(mod)} = \mathbf{B}_{CF} + amt1 \cdot t_1 \cdot \mathbf{B}_{T1}B + t_2 \cdot \mathbf{B}_{T2} + \\ + amr \cdot (s \cdot \mathbf{B}_{SRC} + p \cdot \mathbf{B}_{PRC}) + b_1 \cdot \mathbf{B}_{R1} + \\ + b_2 \cdot \mathbf{B}_{R1} + \varepsilon \cdot \mathbf{B}_{\perp}^{IMF},\end{aligned} \quad (1)$$

where $\mathbf{B}_{CF}$ is the Chapman-Ferraro field, $\mathbf{B}_{T1}$ and $\mathbf{B}_{T2}$ correspond to the inner and outer parts of the cross-tail current, respectively, $\mathbf{B}_{SRC}$ is the contribution from the ring current corresponding to its axially symmetric component, $\mathbf{B}_{PRC}$ is the partial ring current field, $\mathbf{B}_{R1}$ and $\mathbf{B}_{R2}$ are the fields of the Region 1 and 2 Birkeland current systems, and $\mathbf{B}_{\perp}^{IMF}$ is the penetrated component of the IMF.

[19] We varied these free linear parameters (amplitude multipliers of the tail and ring current systems) minimizing the error, which was computed as follows:

$$B\Delta B = \frac{\sqrt{(\mathrm{SymH}^{(mod)} - \mathrm{SymH}^{(obs)})^2 + \sum_{i=1,N}(\mathbf{B}_i^{(mod)} - \mathbf{B}_i^{(obs)})^2}}{N+1}. \quad (2)$$

To obtain a model SymH index, we computed the H-component of the model magnetic field at six ground-based station positions, those used for the real index determination. Then we did the same for the TS05 model with quiet time parameters (P_{sw} = 1 nPa, Dst = 0 nT, IMF B_y = 0 nT, IMF B_z = 2 nT). Model SymH index was computed as following:

$$\mathrm{SymH}^{(mod)} = \frac{\sum_{i=1,6}(B_H - B_{Hquiet})}{0.8\sum_{i=1,6}\cos\alpha_i}, \quad (3)$$

where α_i is the magnetic latitude of the *ith*-station and the factor of 0.8 in the denominator is for ground induced currents.

[20] We also tested the validity of the adjusted models by analyzing the error behavior for various parameters for a few times. We analyzed a subset of free parameters for which the error differed from minimal less than 1 nT (we consider 1 nT as an accuracy of spacecraft magnetic field observations). The minimal and maximal values of the free parameters over this subset were computed and if they differed a lot, it meant that the inverse task was ill-defined. It has been found that for existing configurations of spacecraft during the modeled storm it does not make sense to use more than two free parameters. More parameters do not lead to model quality improvement. Even with only two free parameters, the model can still be ill-defined for some spacecraft configurations.

3.2. Inner Magnetosphere Particle Transport and Acceleration Model

[21] The inner magnetosphere particle transport and acceleration model (IMPTAM), developed by *Ganushkina et al.* [2001, 2005, 2006, 2011], follows distributions of ions and electrons with arbitrary pitch angles from the plasma sheet to the inner L-shell regions with energies reaching up to hundreds of keVs in time-dependent magnetic and electric fields. We trace a distribution of particles in the guiding center, or drift, approximation, in which we can picture the motion of a charged particle as displacements of its guiding center, or the center of the circular Larmor orbit of a moving particle. The guiding center theory assumes that the electromagnetic fields are known and can be used in geophysical plasmas, where the external field is strong and will not be changed much by the motion of the particle themselves.

[22] For the guiding center drifts we take into account $\mathbf{E} \times \mathbf{B}$ drift, where $\mathbf{E}$ and $\mathbf{B}$ are electric and magnetic fields, respectively, and magnetic drift, which, in its turn, includes gradient and curvature drifts. The drift velocity is a combination of the velocity $V_{E\times B}$ due to $\mathbf{E} \times \mathbf{B}$ drift $V_{E\times B} = (\mathbf{E} \times \mathbf{B})/\mathbf{B}^2$ and the velocities of gradient V_∇ and curvature V_{cur} drifts $V_\nabla + V_{cur} = (mv_\perp^2)/(2qB^2)(\mathbf{B} \times \nabla\mathbf{B}) + (mv_\parallel^2)/(qR_c^2B^2)(\mathbf{R_c} \times \mathbf{B})$ [*Roederer*, 1970], where m is the particle mass, q is the particle charge, $v_\perp$ and $v_\parallel$ are the particle velocities perpendicular and parallel to the magnetic field, respectively, and R_c is the radius of curvature of magnetic field line ($\nabla_\perp B = -(B/R_c)\mathbf{n}$, where $\mathbf{n}$ is the unit normal vector along the radius of curvature).

[23] We assume that the first and second adiabatic invariants are conserved. With the above mentioned assumptions, we consider the bounce-average drift velocity after averaging over one bounce of $\mathbf{E} \times \mathbf{B}$ magnetic drift velocities [*Roederer*, 1970, Appendix 2]

$$\langle v_0 \rangle = \frac{\mathbf{E}_0 \times \mathbf{B}_0}{B_0^2} + \frac{2p}{q\tau_b B_0} \nabla I \times \mathbf{e}_0, \tag{4}$$

where $\mathbf{E}_0$ and $\mathbf{B}_0$ are electric and magnetic fields in the equatorial plane, respectively, p is the particle's momentum, τ_b is the particle's bounce period, $I = \int_{S_m}^{S'_m} [1 - \frac{B(s)}{B_m}]^{1/2} ds$, S_m and S'_m are the mirror points, $B(s)$ is the magnetic field along magnetic field line, B_m is the magnetic field at the mirror point, $\mathbf{e}_0$ is the unit vector in the direction of the magnetic field $\mathbf{B}_0$.

[24] Generally, the changes in the distribution function $f(R, \phi, t, E_{kin}, \alpha)$, where R and ϕ are the radial and azimuthal coordinates in the equatorial plane, respectively, t is the time, E_{kin} is the particle energy, α is the particle pitch angle, are obtained by solving the following equation:

$$\frac{df}{dt} = \frac{\partial f}{\partial \phi} \cdot V_\phi + \frac{\partial f}{\partial R} \cdot V_R + sources - losses, \tag{5}$$

where V_ϕ and V_R are the azimuthal and radial components of the bounce-average drift velocity.

[25] At the beginning of modeling with IMPTAM, the inner magnetosphere is considered empty. In this case, only the effects of newly entering particles from the plasma sheet are investigated. The model boundary is set in the plasma sheet at distances, depending on the scientific questions we are trying to answer, from 6.6 R_E to 10 R_E. The particle distribution at the boundary is defined as a Maxwellian or kappa distribution function with parameters obtained from the empirical relations or from the observations during specific events.

[26] Liouville's theorem states that, in the absence of external forces and losses, the distribution function remains constant along the dynamic trajectory of particles. This theorem is used to gain information of the entire distribution function. If we know the distribution function $f(R, \phi, t, E_{kin}, \alpha)$ of particles at a time moment t_1, then we can obtain the distribution function of particles at a time moment $t_2 = t_1 + \Delta t$, by computing the drift velocity of the particles. The distribution function at t_2 will not be the same as at t_1 at the corresponding positions, since we need to take into account the phase-space-dependent losses (τ_{loss}). The final distribution function at t_2 will be $f(t_2) = f(t_1)\exp(-\frac{\Delta t}{\tau_{loss}})$.

[27] Particle loss processes, which are important for modeling the ring current ions, include charge-exchange with neutral hydrogen in the upper atmosphere, Coulomb collisions, and convective outflow through the magnetopause. The charge-exchange cross-section is obtained from *Janev and Smith* [1993]. The thermosphere model MSISE 90 [*Hedin*, 1991] and the plasmasphere model by *Carpenter and Anderson* [1992] are used.

4. Modeling of Inner Magnetosphere Current Systems With Magnetic Field Models

4.1. Configuration of Available Satellites

[28] During the July 21–23, 2009 time interval several satellites were passing the inner magnetosphere regions, such as two geostationary GOES 11 and 12, four THEMIS A, C, D, and E, and Cluster. We set the inner magnetosphere region to be within 15 R_E on X_{GSM}, Y_{GSM} and Z_{GSM}. We also have checked that the satellites were inside the dayside magnetopause. Times of crossing the magnetopause were seen in the magnetic field observations as sharp jumps in magnetic field components. Figure 2a shows the orbits of satellites in MLT(UT) format, which were in the inner magnetosphere regions and whose magnetic field data were available. The MLT- and UT-coverage varied throughout the storm. Figure 2b presents the measured SymH index.

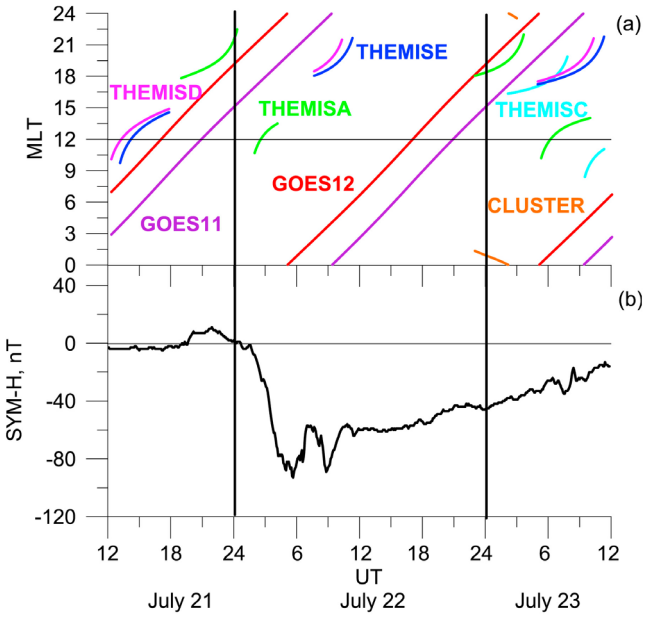

Figure 2. (a) Orbits of available satellites in MLT(UT) format for the July 21–23, 2009 storm together with (b) measured SymH index.

[29] During the storm initial phase on July 21, 2009, both GOES spacecraft were on the dayside, moving from dawn to dusk. THEMIS A was on the duskside moving toward midnight but close to the Earth ($X_{GSM} = -2\ R_E$). It was near the equatorial plane but coming from the flank on the dusk side, so only the data from the part of the orbit at the end of the day (19–24 UT) could be used. THEMIS D and E were on the dayside, going from dawn to dusk, and the data were available for the part of the day, from 12 to 18 UT. There was a lack of nightside measurements for the first day of the storm.

[30] For the storm main phase on July 22, 2009, more satellites were on the nightside including both GOES craft and THEMIS D and E. THEMIS D and E were on the duskside coming from the flank (from $Y_{GSM} = 10\ R_E$) toward midnight, close to the Earth ($X_{GSM} = -2\ R_E$) and to the equatorial plane and the data were available during 07–11 UT, which is after the first drop in the Dst index but during the storm main phase. THEMIS A was on the dayside and only data from the first 4 hours of July 22nd could be used. Thus, no data beyond the geosynchronous orbit on the nightside were available for the storm main phase.

[31] On July 23rd in addition to GOES 11 and 12, and THEMIS A, D, and E, THEMIS C and Cluster happened to be inside the inner magnetosphere region. Both GOES spacecraft were on the nightside in the beginning of the recovery phase on July 23rd. Cluster was on the nightside crossing in X_{GSM} from -9 to $-4\ R_E$ but rather far below the equatorial plane with Z_{GSM} of $-7\ R_E$. Data from two parts of the orbits of THEMIS A (00–04 UT and 05–10 UT) and THEMIS C (02–07 UT and 09–11 UT) were used. On the first parts of their orbits, THEMIS A was on the nightside near dusk but close to Earth, and THEMIS C was on the duskside going from day to night. On the second parts, both THEMIS A and THEMIS C were on the dayside. THEMIS D and E were located similar to July 22nd, on the duskside coming from the flank (from $Y_{GSM} = 10\ R_E$) toward midnight, close to the Earth ($X_{GSM} = -2\ R_E$) and equatorial plane. Data were available during 05–11 UT.

[32] This configuration of satellites lacks the data from the nightside but it is the best available for the first storm in 2009, which occurred after a rather long quiet period.

4.2. Magnetic Field in the Inner Magnetosphere During Storm Main Phase on July 22, 2009: Observations and Modeling

[33] The magnetic field components measured at the satellites shown in Figure 2a were compared with modeled values from four different magnetic field models for the storm period on July 21–23, 2009. Figure 3 demonstrates how well different models can follow the observed magnetic field components (black lines) at GOES 11 (Figures 3a–3c), GOES 12 (Figures 3d–3f), THEMIS D (Figures 3g–3i) and THEMIS E (Figures 3j–3l) during the main phase of the storm on July 22nd. The models used for comparison are T96 (blue lines), T02 (purple lines), TS05 (green lines), and TS05m (red lines). GOES 11 and 12 data were available for the whole day of July 22nd. As can be seen, the TS05m model best described the observed geostationary magnetic field components among the models, in general. There is a recognizable difference between T96 and other models. The storm event was small so that even the modified best-fit TS05m model gave rather small improvements compared to the standard model TS05. THEMIS D and E data [*Auster et al.*, 2008] were available only for a short period between 07 and 11 UT on July 22nd, when both spacecraft were on the duskside. For THEMIS D data, TS05m fitted the observed B_x- and B_z-components best but none of the models was able to follow the B_y-component. For THEMIS E data, both the B_y and B_z-components are not reproduced by any of the models.

[34] Figure 4 presents the error estimates for all models. The first three panels from the top show the errors between the modeled and observed magnetic field at the satellites $error\ s/c = \frac{\sqrt{\sum_{i=1,N}(\mathbf{B}_i^{(mod)} - \mathbf{B}_i^{(obs)})^2}}{N}$ (Figure 4a), between the modeled and observed SymH index $error\ SymH = |SymH^{(mod)} - SymH^{(obs)}|$ (Figure 4b), and the total error ΔB (equation (2)) (Figure 4c). Lines for different models are shown with the same color as in Figure 3. The number of satellites the data were available from, as dependent of time, is shown in Figure 4e.

[35] Among the four models, T96 gives the largest errors and TS05m gives the smallest errors. After 07 UT on July 22nd, the errors at satellites and total errors from T02, TS05 and TS05m models do not differ much (Figures 4a and 4c). For the SymH error (Figure 4b), the TS05m model has the smallest error. As can be seen, the main difference in model errors occurs at the main phase of the storm during the first dip in the SymH index, presented in Figure 4d as the black line. Even though TS05m model exhibits the smallest errors, the errors for all models including TS05m are rather large (20–50nT) during the first part of the storm main phase (03–07 UT on July 22nd). It should also be kept in mind that the data from two GOES satellites, though on the nightside, were available for this time period with THEMIS A data

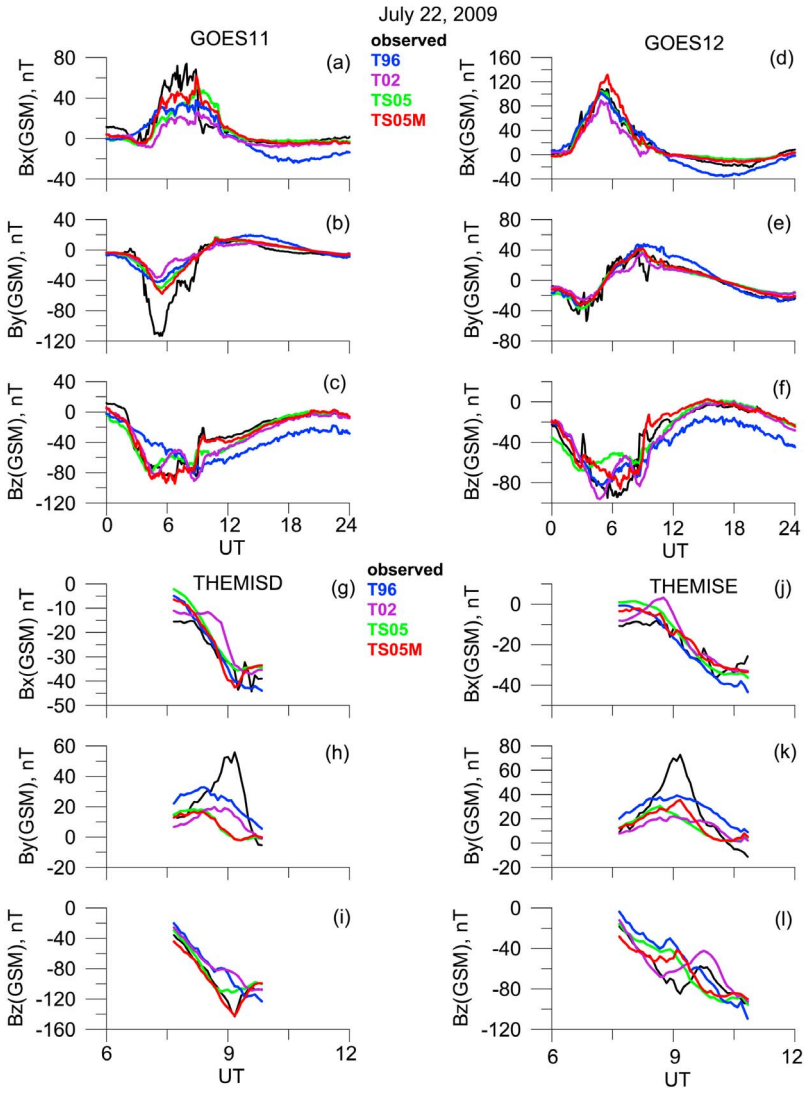

Figure 3. Measured and modeled magnetic field at GOES 11 and 12 and THEMIS D and E satellites during July 22, 2009.

only for a short interval, when SymH started to drop (Figures 4d and 4e). At any case, we can not say that using TS05m model for this particular storm was a significant improvement as compared to the standard TS05 model.

[36] Figure 4d demonstrates how the two parameters, namely, the amplitudes for the ring (*amr*, orange line) and tail (*amt*1, light blue line) current systems, introduced in the TS05m model, varied with time. If the amplitude is close to 1, it means that no modifications were done to the standard representation of the ring and tail current systems in TS05. Values above and below 1 mean an increase or decrease of the standard currents, respectively. During the first dip in SymH, the model tail current was almost twice larger than the standard one, whereas the model ring current was set too small. Detailed analysis has shown that the algorithm of TS05m gives an unstable result for this period with such sparse data. Figure 4d demonstrates the uncertainty of the TS05m results, where one can see an oscillation of the ring current amplitude at July 22, 04–08 UT. The specifications of the ring and tail currents are not fully correct and defined for the modeled period for this satellite configuration. The model can give an increase of the tail current with a simultaneous decrease of the ring current or vice versa trying to fit the magnetic field measurements. As a result of this analysis, it became clear that our attempts to use the adaptive modeling approach did not provide a better model than the standard TS05 for this particular storm. Further in this paper we will use the standard TS05 model to analyze the relative behavior of the ring and near-Earth tail current systems during the small HSS/CIR storm on July 21–23, 2009.

4.3. Equatorial Current Densities

[37] To study the behavior of the ring and near-Earth tail current systems during the July 21–23, 2009 storm, we computed the total current densities using the magnetic field given by the TS05 model. Figure 5 presents the current densities in nA/m^2 in the equatorial plane on July 22, 2009 for six time moments, such as at the storm initial phase

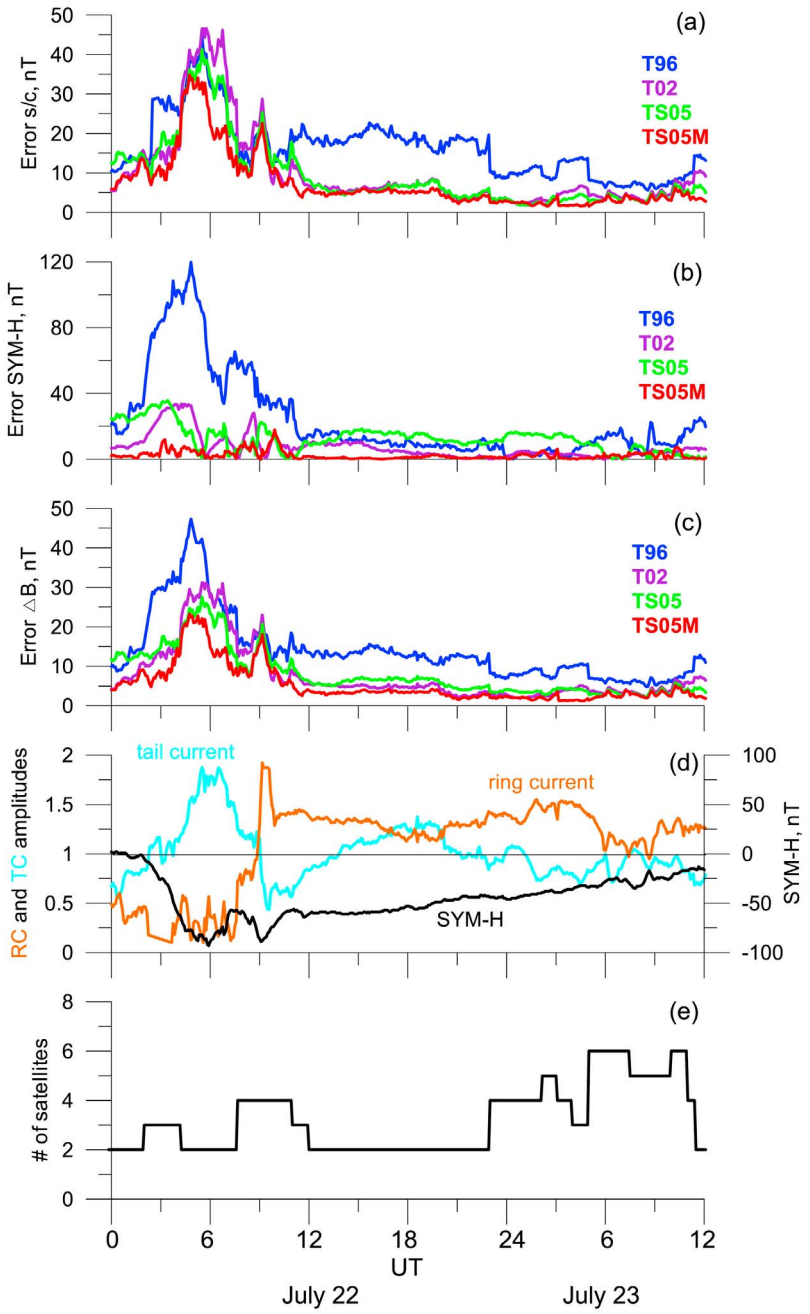

Figure 4. Estimated errors for magnetic field models (a) between the modeled and observed magnetic field at the satellites, (b) between the modeled and observed SymH index, and (c) the total error ΔB, (d) amplitudes for the ring (*amr*) and tail (*amt*1) current systems, introduced in the TS05m model, together with measured SymH, (e) number of satellites, the data were available from, during July 22–23, 2009.

(00 UT) (Figure 5a), storm main phase (04 UT) (Figure 5b), time of the first minimum in the SymH index (O6 UT) (Figure 5c), peak recovery after that first minimum (08 UT) (Figure 5d), second minimum of SymH (0915 UT) (Figure 5e), and storm recovery (18 UT) (Figure 5f). The directions of currents are shown by white arrows on the images which are the projections of current vectors of unit length onto the XY-plane. The arrows allow us to determine whether the model currents are closed on the magnetopause or go around the Earth. Ten times increase can be seen in the ring and near-Earth currents during the storm main phase. The ring current was more intense with densities reaching 24 nA/m^2 during this storm than the tail current with about 16 nA/m^2. Another characteristic feature is that the ring current, being asymmetric during the storm main phase and symmetrizing during the storm recovery phase, did not show a duskward shift of its peak during considered time interval. Although the TS05 model included a possibility of a rotation of the model partial ring toward the duskside by an angle, depending on the storms intensity and phase, this angle was fixed in the actual model. The tail current did

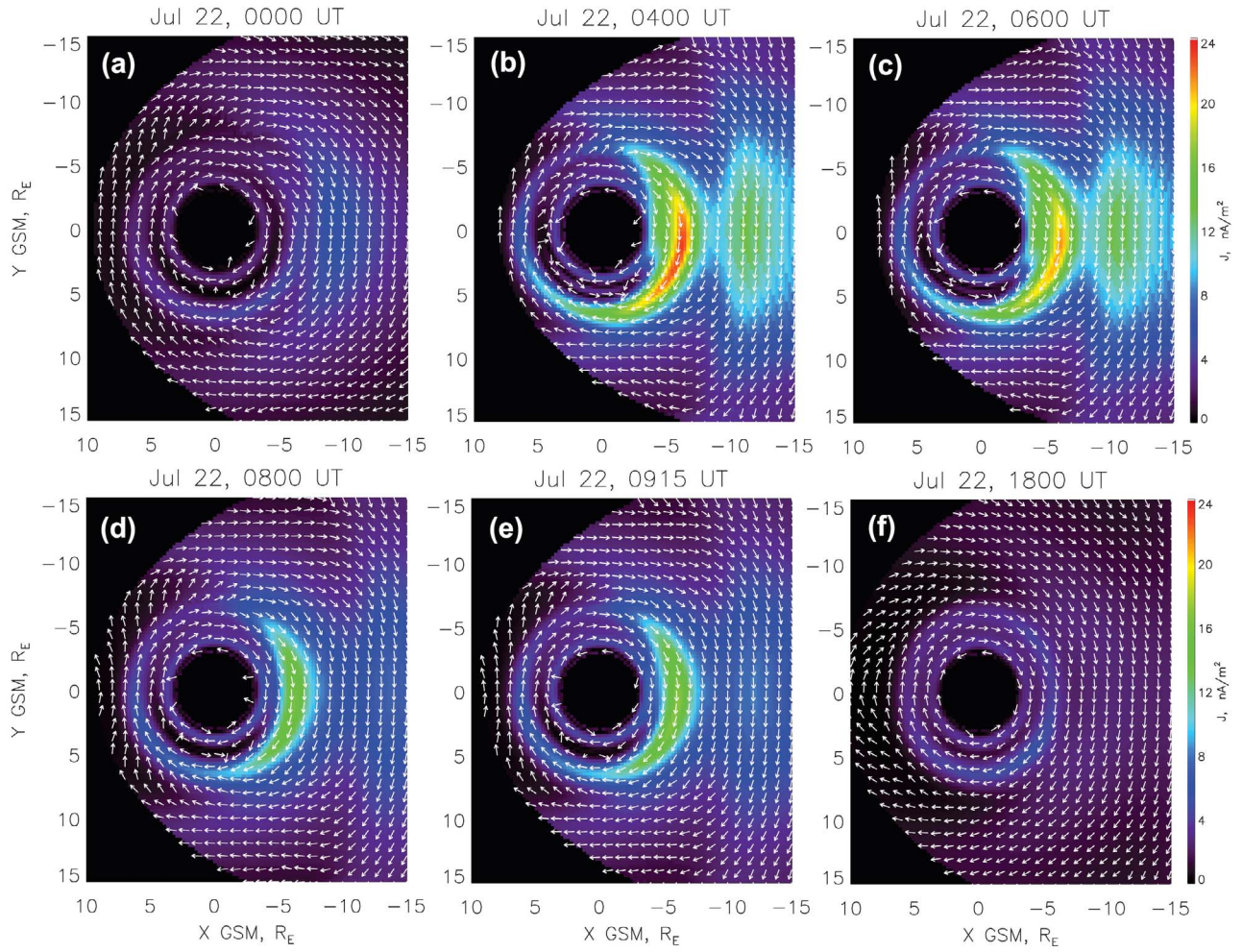

Figure 5. (a–f) Current densities in nA/m^2 in the equatorial plane computed with the TS05 model for July 22, 2009 together with directions of currents shown by white arrows.

not show any intensifications during the second dip in SymH (0915 UT) but decreased. The ring current was two times more intense than the tail current. The separation between the ring and tail currents was assumed based not only on the locations in X_{GSM} of current density peaks but also on the directions of the current vector.

4.4. Contributions From the Ring and Tail Currents to the SymH Index

[38] In addition to analyzing the evolution of current densities during the storm on July 21–23, 2009, the contributions to the SymH index from the ring and tail current systems were calculated using the TS05 model. Figure 6 shows the observed SymH index (thin black line), the model total SymH index (thick black line), and the contributions from the ring (orange line) and tail (light blue line) current modules as given by the TS05 model. The observed and modeled SymH indices have contributions from all current systems but with that of the induced currents removed (assumed to be 25%) for the observed SymH and not included for the model SymH (equation (3)). The contributions from the ring and tail currents were calculated using the magnetic field from their modules only in the TS05 model.

[39] The modeled SymH index does not follow the shape of the observed one. At the same time, it shows the existence of two minima and fit the first minimum by magnitude but not by time. As can be seen, the main contribution comes from the tail current module (from about 75 nT of total SymH, 62 nT comes from the tail current during the first minimum of SymH). The tail current module starts to develop earlier, it follows the model total SymH index during its first drop. The ring current module contributes only 30 nT to 75 nT of the total SymH at the first minimum. The tail current module recovers faster than the ring current module, the ring current module contributes more only during the storm late recovery. This behavior is very typical when TS05 [*Tsyganenko and Sitnov*, 2005] or later versions [*Sitnov et al.*, 2010] of the Tsyganenko model are used.

[40] If we compare the behavior of the ring and tail current systems seen as contributions to the SymH index and as evolution of current densities in the equatorial plane shown in Figure 5, the dominant role of the tail current becomes questionable. As can be seen in Figure 5, the ring

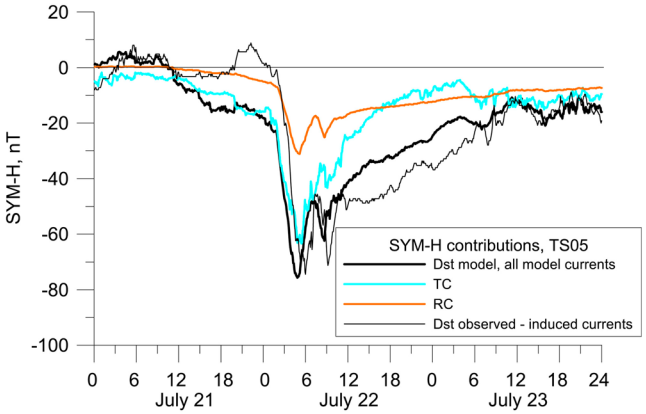

Figure 6. Contributions to the SymH index calculated with the TS05 model from the ring (orange line) and tail (light blue line) currents and the observed SymH index (thin black line) and model total SymH index (thick black line) for July 21–23, 2009.

current is more intense than the tail current during the storm main phase.

[41] In order to study the question of tail current contribution to the SymH index, we performed calculations of the total current lines as lines with the direction of the total current density vector tangential to them by the TS05 model and determined the regions of the different types of these current lines. Figure 7 presents the locations of three types of current lines in the midnight meridional plane, shown by plus signs with different colors together with the current density of the tail current module only computed using TS05 with quiet time parameters (P_{sw} = 1 nPa, Dst = 0 nT, IMF B_y = 0, IMF B_z = 2 nT) (Figure 7a),storm main phase (04 UT) (Figure 7b), and the time of the first minimum in the SymH index (06 UT) on July 22, 2009 (Figure 7c).

[42] Current lines were computed as lines with the direction of the TS05 total current density vector tangential to them. Tracing of current line required the double precision version of TS05 model. To estimate the current density vector from the model magnetic field, we used the finite differences on the scale of 0.0001 R_E for the estimate of the $\nabla \times \mathbf{B}$ ($curl\mathbf{B}$). For current line tracing we used a Runge-Kutta 4th order method with fixed stepsize of 0.005 R_E. Since this procedure of tracing of current lines are rather time-consuming, we set zero dipole tilt angle and used mirror symmetry relative to Z_{GSM} = 0 plane to trace only the current lines in the $Z_{GSM} \geq 0$ region. At first, we selected the region of the midnight meridian plane confined inside the expected separatrix between closed and open current lines. The boundaries of this region are shown by white solid lines in all panels in Figure 7 which were determined approximately by examining the current density distributions.

[43] We defined a grid on the XZ-plane at midnight with Y_{GSM} = 0 with 0.1 R_E step in X_{GSM} and 0.05 R_E step in Z_{GSM}. From each grid point at midnight we follow a current line in both directions, to positive and negative Y_{GSM} or to dawn and dusk. The current lines which end up having both ends on the magnetopause are marked with white plus signs. If both ends of a current line go around the Earth and cross the dayside meridian, this line is shown by the black plus sign in Figure 7. Red pluses correspond to the current lines with both ends coming to the Earth. For simplicity we considered a sphere with radius of 2.5 R_E as an Earth's surface. Only these three types of current lines are presented in Figure 7. All the others were ignored and not shown in Figure 7, which resulted in the existence of the areas without any signs. It must be stresses that the distribution of current density shown by color is from two tail current modules of TS05 only (equation (1)), but current from all TS05 modules was used for tracing the current lines.

[44] For quiet conditions (Figure 7a), the peak of the current density of the tail current module was located around $X_{GSM} = -10\ R_E$. The location of the tail current was consistent with the area occupied by white plus signs. The current lines had both ends on the magnetopause, which corresponds to the definition of the tail current in the nightside plasma sheet. A large area earthward from the tail current from -8 to $-4\ R_E$ in X_{GSM} is covered by black pluses indicating current flowing around the Earth. As can be seen, the tail current density is not zero (0.5–1 nA/m^2) in

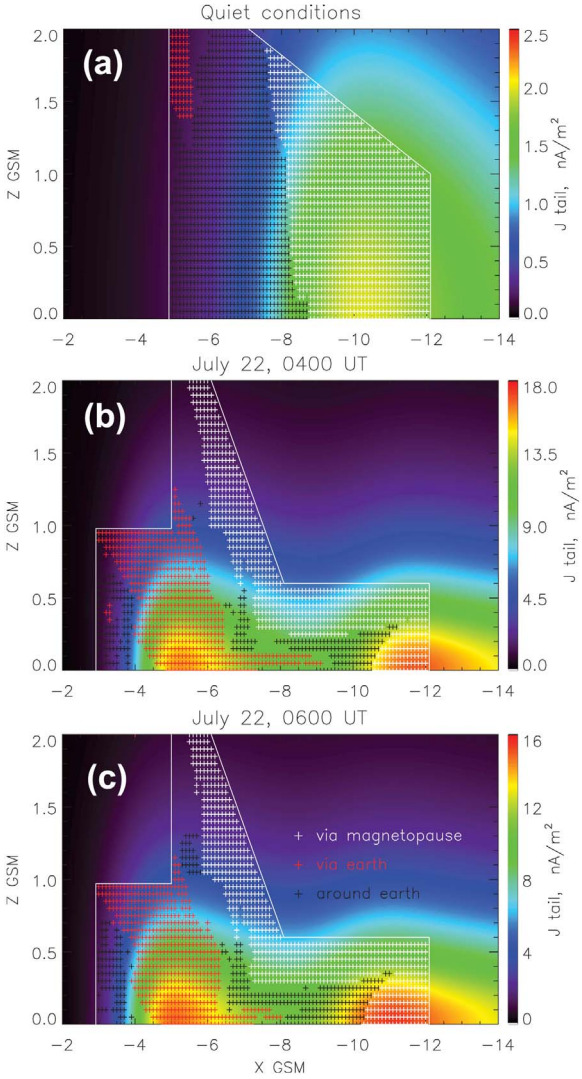

Figure 7. (a–c) Current densities of the TS05 tail current only together with regions of current lines for current from all TS05 modules for July 22, 2009 (see text).

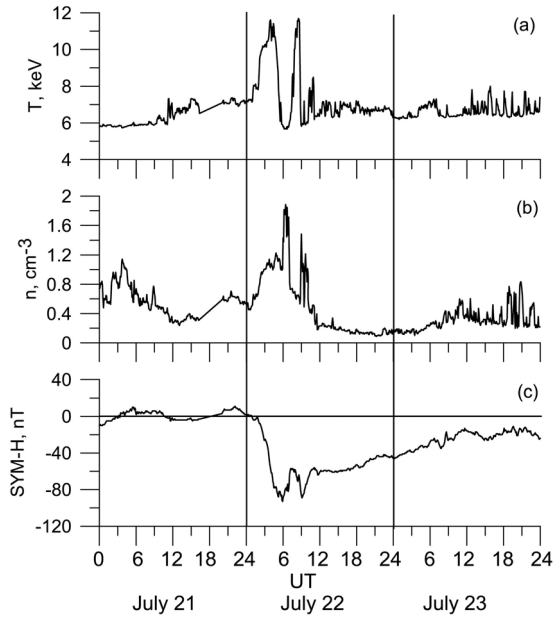

Figure 8. (a–c) Boundary conditions given by the empirical model derived from Geotail data by *Tsyganenko and Mukai* [2003] used for particle modeling with IMPTAM for the July 21–23, 2009 storm.

this area. A small region of red pluses around $X_{GSM} = -5\ R_E$ and $Z_{GSM} = 1.5$–$2\ R_E$ can be related to the small part of the current which is connected with the ionosphere by field-aligned current, most evidently, in the Region 2 sense.

[45] In the beginning of the storm main phase (Figure 7b), the tail current density shows the appearance of a second peak at about $X_{GSM} = -5\ R_E$. The first peak moved tailward to $X_{GSM} = -12\ R_E$. The earthward peak coincides with the area of current lines with both ends at the Earth's surface. Earthward from this peak (from $X_{GSM} = -4\ R_E$), the current lines go around the Earth. The region from -7 to $-10\ R_E$ in X_{GSM} also corresponds to the current lines going around the Earth and crossing the dayside meridian. It is located between two peaks of the tail current density. The current lines with both ends on the magnetopause occupy the area of the tailward peak and above the equatorial plane with Z_{GSM} from 0.3 to 2 R_E earthward up to about $-6\ R_E$.

[46] For the storm main phase maximum (Figure 7c) the locations of the tail current densities and areas of current lines do not change much. The tail current density peaks are wider and more intense.

[47] As can be noted from Figure 7, the current lines computed using TS05 model for the storm main phase can be attributed to the (1) symmetric ring current flowing at distances earthward of $-4\ R_E$, then to the (2) asymmetric current with closure via Region 2 field-aligned currents at X_{GSM} from -4 to $-6\ R_E$ with Z_{GSM} up to 1.2 R_E, then again (3) symmetric ring current at X_{GSM} from -6 to $-10\ R_E$, flowing not far from the equatorial plane (small Z_{GSM}) and, finally, the (4) tail current at X_{GSM} from -10 to $-12\ R_E$ near the equatorial plane and also earthward up to $X_{GSM} = -5\ R_E$ above the equatorial plane. At the same time, the peaks in the tail current density do not always correspond to the current lines having both ends at the magnetopause. Moreover, the tail current has a peak in the region, where current lines do not go to the magnetopause but look more like ring current. Therefore, when calculating the contributions from the tail currents to the SymH index from the tail current module in the TS05 model (Figure 6), the contributions from other current systems than those which have both ends at the magnetopause are included. The dominant tail current contribution seen in Figure 6 during the main phase of July 21–23, 2009 storm can be largely overestimated.

5. Modeling of Inner Magnetosphere Current Systems With IMPTAM Model

[48] In addition to magnetic field modeling made with the TS05 model, we also performed particle modeling with IMPTAM for the July 21–23, 2009 storm in order to study the evolution of the ring and near-Earth tail current systems. We set the IMPTAM boundary at 10 R_E on the nightside and define a Maxwellian proton distribution function there with the parameters, such as plasma sheet temperature T and number density n given by the empirical model derived from Geotail data by *Tsyganenko and Mukai* [2003]. In the work by *Tsyganenko and Mukai* [2003], both plasma sheet temperature T and number density n depend on the solar wind velocity and IMF B_z. Number density n depends also on the solar wind number density. Figure 8 shows the variations of temperature T (Figure 8a) and number density n (Figure 8b) at 10 R_E in the plasma sheet for July 21–23, 2009 storm together with the observed SymH index (Figure 8c). The plasma sheet temperature reaches 12 keV and the number density reached 1.9 cm^{-3} during the storm main phase.

[49] At the beginning of IMPTAM simulations, the inner magnetosphere is considered empty. In this case, only the effects of newly entering particles from the plasma sheet are investigated. The preexisting particles are subject to loss quickly after the newly injected particles populate the inner magnetosphere [*Kozyra et al.*, 2002; *Ganushkina et al.*, 2006]. We follow protons in the TS05 magnetic field model, which is the same as we have used for our magnetic field modeling presented in the previous sections of this paper. For the electric field we use the *Boyle et al.* [1997] polar cap potential dependent on solar wind and IMF parameters applied to a Volland-Stern [*Volland*, 1973; *Stern*, 1975] type convection electric field in the magnetosphere. Although IMPTAM does take into account the self-consistency of the magnetic field by calculating the magnetic field produced by the model currents and feeding it back to the background magnetic field, we do not use this feature in the present study. Using a realistic model magnetic field such as Tsyganenko models, where there are prescribed ring and near-Earth tail currents, together with calculations of the induced magnetic field to trace particles in them, results in incorrect results [*Ganushkina*, 2011]. To be accurate, it is necessary to remove the model ring and near-Earth tail currents from the background magnetic field model and consider self-consistent calculations of the magnetic field. For the present study the idea was to use the same magnetic field model for the particle modeling as was used for magnetic field modeling.

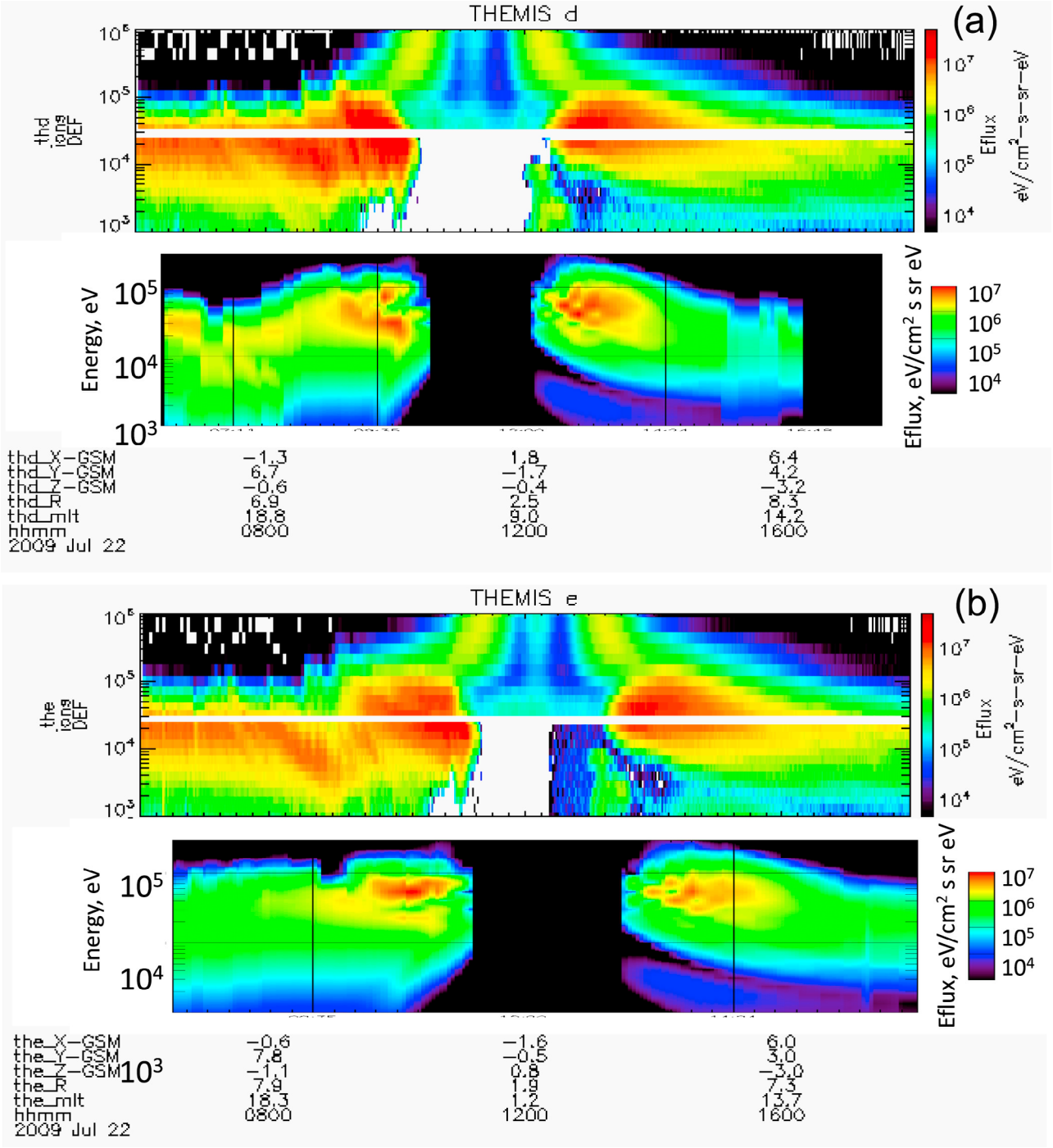

Figure 9. (a–b) Energy flux measured on THEMIS D and E satellites from 06 UT to 18 UT on July 22nd, 2009 compared to the model spectrograms of IMPTAM fluxes.

[50] We calculate the model SymH index by using the Biot-Savart law to derive the magnetic disturbance induced by the current. The current density $\mathbf{J}_\perp$ perpendicular to the magnetic field $\mathbf{B}$ is given by

$$\mathbf{J}_\perp = \frac{\mathbf{B}}{B^2} \times [\nabla P_\perp + (P_\parallel - P_\perp)\frac{(\mathbf{B}\cdot\nabla)\mathbf{B}}{B^2}], \quad (6)$$

where $P_\parallel$ and $P_\perp$ are plasma pressure, parallel and perpendicular to the magnetic field. The magnetic disturbance parallel to the Earth's dipole at the center of the Earth $\triangle B$ is induced by the azimuthal component J_ϕ of $\mathbf{J}_\perp$

$$\Delta B = \frac{\mu_0}{4\pi}\int_r\int_\lambda\int_\phi \cos^2\lambda J_\phi(r,\lambda,\phi)drd\lambda d\phi, \quad (7)$$

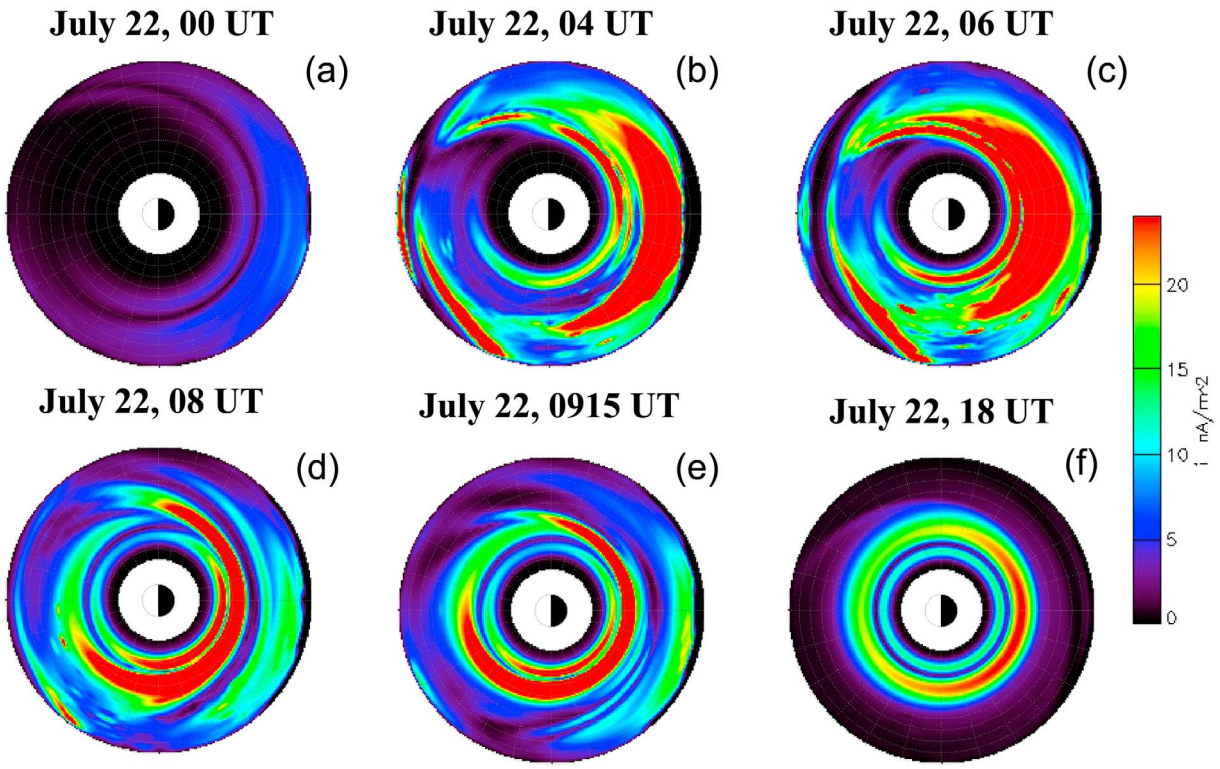

Figure 10. (a–f) Current densities in nA/m^2 in the equatorial plane computed with IMPTAM for July 22, 2009.

where μ_0 is the magnetic permeability, r is the radial distance, λ is the latitude, ϕ is the MLT and J_ϕ is given by

$$J_\phi = \frac{1}{B^2}\left(\frac{B_r}{r}\frac{\partial P_\perp}{\partial \lambda} - B_\lambda \frac{\partial P_\perp}{\partial r}\right) + \frac{1}{B^3}(P_\parallel - P_\perp)\left(\frac{B_r}{r}\frac{\partial B}{\partial \lambda} - B_\lambda \frac{\partial B}{\partial r}\right) \quad (8)$$

and ΔB is an estimate of the pressure-corrected *Dst* index without the contribution from the Earth's induced currents.

5.1. Comparison With THEMIS Spectrograms

[51] In order to test the ability of the IMPTAM to model the particle fluxes in the inner magnetosphere, the comparisons with the observed energy-time ion spectrograms were made. The exact similarity of the model and the observed spectrograms was not the goal of this test. For this test we used in situ ion data from THEMIS satellites. For the storm main phase on July 22, 2009, THEMIS D and E were on the duskside coming from the flank (from $Y_{GSM} = 10\ R_E$) toward midnight, close to the Earth ($X_{GSM} = -2\ R_E$) and were near the equatorial plane and the data were available during 07–11 UT, which is after the first drop in the SymH index but during the storm main phase. We used the data from the solid state telescope (SST) and electrostatic analyzer (ESA) [*Angelopoulos*, 2008; *McFadden et al.*, 2008] which measure ion distribution functions in energy ranges of 5 eV to 25 keV (ESA) and 30 keV to 1 MeV (SST).

[52] Figure 9a (top), shows the energy flux measured by ESA and SST on the THEMIS D satellite from 06 UT to 18 UT on July 22nd, 2009. There is a data gap at 20 to 30 keV in the spectrogram which corresponds to the real gap between energy ranges of the two instruments. A b-nose structure [*Smith and Hoffman*, 1974; *Ejiri et al.*, 1980; *Ganushkina et al.*, 2001; *Buzulukova et al.*, 2003] can be seen at the inbound pass with characteristic energy of about 20 keV. THEMIS D was in the afternoon sector on the outbound pass, so a "gap" [*Shirai et al.*, 1997; *Sauvaud et al.*, 1998; *Buzulukova et al.*, 2002] is present in the spectrogram at lower energies of about 10 keV. Figure 1b (top) shows the energy flux measured by ESA and SST on the THEMIS E satellite from 06 UT to 18 UT on 22 July 2009. Since THEMIS E was on an orbit, close to that of THEMIS D, its spectrograms contain similar features as those observed by THEMIS D.

[53] Figures 9a and 9b, lower panels, present model spectrograms of IMPTAM fluxes along THEMIS D and THEMIS E orbits, respectively, for 06–18 UT on July 22nd, 2009. Since this comparison is a test for IMPTAM fluxes for the modeled storm, we can say that the main features of the observed spectrogram, such as maximum flux values (about 10^7 *eV/cm^2 sr s eV*), nose structure and ion gap are reproduced reasonably well. This gave us a confidence that IMPTAM can be used for modeling the current densities and Dst index during the CIR/HSS storm on July 21–23, 2009 for further comparison with the magnetic field modeling presented above.

5.2. Equatorial Current Densities

[54] To study the behavior of the ring and near-Earth tail current systems during the July 21–23, 2009 storm, we computed the total current densities using IMPTAM. Similarly to Figure 5, Figure 10 presents the current densities in

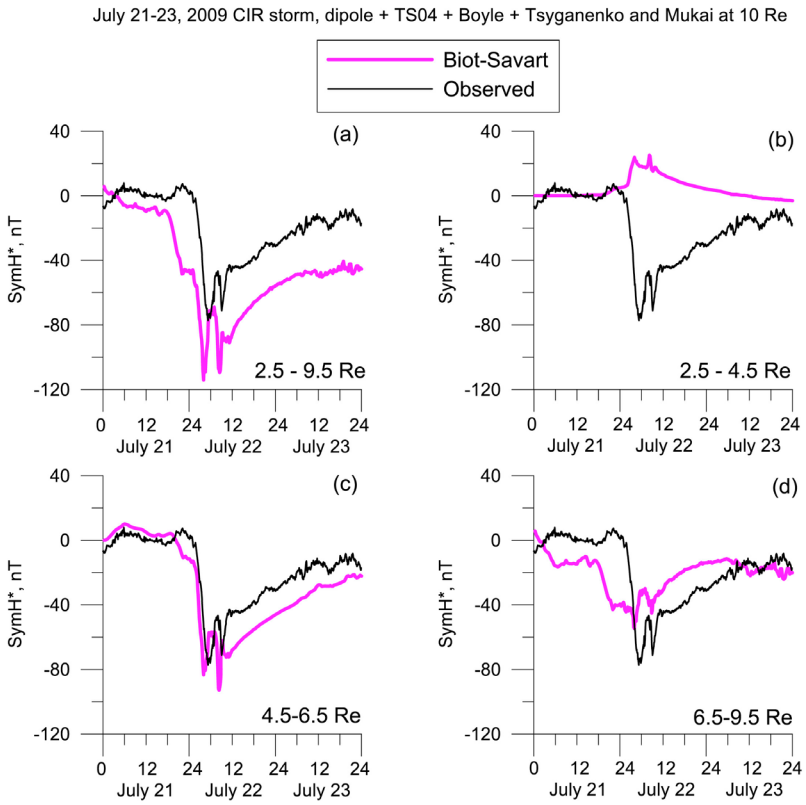

Figure 11. "Contributions" to the modeled by IMPTAM SymH (pink lines) calculated using Biot-Savart's law for the regions: (a) inside the modeling region of 2.5–9.5 R_E, (b) inside 2.5–4.5 R_E, which roughly corresponds to the eastward ring current, (c) inside 4.5–6.5 R_E, which is assumed to be ring current, and (d) inside 6.5–9.5 R_E, which represents the near-Earth part of the tail current. Pressure-corrected SymH* index with induced currents removed is shown by black lines.

nA/m^2 in the equatorial plane on July 22, 2009 for six time moments, such as at the storm initial phase (00 UT) (Figure 10a) , storm main phase (04 UT) (Figure 10b), time of the first minimum in the SymH index (O6 UT) (Figure 10c), peak recovery after that first minimum (08 UT) (Figure 10d), second minimum of SymH (0915 UT) (Figure 10e), and storm recovery (18 UT) (Figure 10f). The current densities computed using equation (6) are shown for radial distances from 2.5 to 9.5 R_E. Many smaller patches in the current density distribution are the result of calculations using equation (6) and appearances of plasma pressure increases and decreases due to incoming particles from source variations.

[55] The magnitudes of current densities computed with IMPTAM are comparable to those computed with the TS05 magnetic field model (Figure 5). A ten times increase can be seen in the near-Earth currents during the storm main phase. We see the formation of the eastward ring current close to the Earth and a very intense partial ring current (Figures 10b and 10c) which starts to symmetrize at 08 UT (Figure 10d) and becomes symmetric during the recovery phase (Figure 10f). The characteristic feature that the ring current did not show duskward shift of its peak at any time moment during the storm main phase is present here too as compared to Figure 5. We can not make any direct comparisons for the tail current since our boundary was set at 10 R_E.

5.3. SymH-"Contributions"

[56] In addition to analyzing the evolution of current densities during the storm on July 21–23, 2009, the "contributions" to the SymH index from the ring and tail current systems were calculated using IMPTAM. In reality, it is not straightforward to compute the contributions in a similar way as it was done in Figure 6 or easily determine the current lines and perform integrations inside the regions occupied by different current systems. Instead, we adopted rather simple way to define the current system regions. To obtain the total model SymH index, we used equation (7) for the modeling region inside 2.5–9.5 R_E. It is shown in Figure 11a by a pink line. It contains the contributions from all model current systems with the induced current not taken into account. We compare it with the observed, pressure-corrected ($SymH^* = SymH - 7.26\sqrt{P_{sw}} + 11.0$ with removed influence of the magnetopause currents ($7.26\sqrt{P_{sw}}$), and a quiet time offset value (11.0 nT) also taken into account) 1 minute SymH* index (black lines), where the induced currents were removed (assumed to be 25%). We can see that the model SymH obtained with particle tracing in TS05 magnetic field and *Boyle et al.* [1997] electric field and *Tsyganenko and Mukai* [2003] boundary conditions underestimated by two times the observed SymH-index. At the same time, the shape of the SymH curve is similar to that observed. This is consistent with previous studies by

Ganushkina et al. [2011]. We divided the modeling region into three regions: (1) inside 2.5–4.5 R_E, which roughly corresponds to the eastward ring current, (2) inside 4.5–6.5 R_E, which is assumed to be ring current and (3) inside 6.5–9.5 R_E, which represents the near-Earth part of the tail current. It must be noted that these divisions are rather crude, and they and the current distinctions are just zero approximation estimates. In IMPTAM modeling it is impossible to state that 6.5–9.5 R_E region contains the tail current but this is the region, where $\mathbf{E} \times \mathbf{B}$ drift is strong and the magnetic drift just starts to become important.

[57] Figure 11b shows the "contribution" from the eastward ring current, it is positive and is about 20 nT at storm maximum. Figure 11c presents the "contribution" from the ring current. For this modeling, the ring current is a major source of the model SymH index. At the same time, the near-Earth tail current (Figure 11c) also has its "contribution" and it is about 40 nT in 80 nT of the observed peak value. The near-Earth tail current starts to develop earlier but also recovers earlier than the ring current. This is very consistent with previous modeling using the event-oriented magnetic field model [*Ganushkina et al.*, 2004].

[58] These patterns of different contributions agree well with the results obtained using the magnetic field modeling presented in Figures 5 and 7. It stresses the importance of including the near-Earth tail currents in the calculations of model SymH or Dst indices. Moreover, it confirms the significance of the way how the model SymH or Dst is calculated, by defining the regions which contain the current systems or by the current representations in the models.

6. Discussion

[59] We presented the results of the modeling of two main current systems, the ring current and the near-Earth tail current, using two different approaches. The first approach was to determine the current systems from the magnetospheric magnetic field models and the second was to use particle transport modeling from the plasma sheet to the inner magnetosphere regions. The focus was set at the behavior of the ring and near-Earth tail currents and their contributions to the SymH index during one particular CIR/HSS-driven storm on July 21–23, 2009.

[60] We tried to follow our previously quite successful modeling efforts [*Ganushkina et al.*, 2004; *Kubyshkina et al.*, 2009] in modifying the standard Tsyganenko models for the magnetospheric magnetic field. Modifications of the TS05 model were made, where two variable multipliers to current systems, such as *amt*1 to the amplitude of the tail (short) module and *amr* to the ring current module amplitudes, were introduced. As a result of the analysis of model errors (Figure 4), it became clear that our attempts to introduce the modifications did not provide a better model than the standard TS05 for this particular storm. The configuration of the satellites was such that not much data from the nightside were available, especially during the storm main phase. For that configuration of spacecraft, it did not make sense to use more than two free parameters. Use of a higher number of free parameters did not lead to the improvement of the quality of the model. Even with only two free parameters, the model can still be ill-defined for some spacecraft configurations. This does not mean that the modifications are incorrect in general but it can mean that the specifications of the ring and tail currents in the model are not fully correct and defined for the modeled period for this satellite configuration. The model can give an increase of the tail current with simultaneous decrease of the ring current or vice versa trying to fit magnetic field measurements.

[61] Equatorial current densities computed by TS05 model and IMPTAM showed rather similar features (Figures 5 and 10). The models are different, although the TS05 model was used in IMPTAM for the background magnetic field. The magnitudes of current densities computed with IMPTAM are comparable to those computed with the TS05 magnetic field model. More than a factor of ten increase was seen in the ring and near-Earth currents during the storm main phase. Another characteristic feature is that the ring current, being asymmetric during the storm main phase and symmetrizing during the storm recovery phase, did not show a duskward shift of its peak during considered time interval. For the TS05 model, this can be attributed to the fixed rotation angle of the model partial ring toward the duskside. The same argument cannot be used for the IMPTAM results. The duskward shift of the partial ring current during storm maximum was obtained from many modeling efforts [*Fok et al.*, 2003; *Jordanova et al.*, 2006; *Liemohn et al.*, 2001; *Ebihara and Ejiri*, 2000; *Ganushkina et al.*, 2005], although other models show no duskward shift or even a dawnward shift [*Ebihara and Fok*, 2004; *Liemohn et al.*, 2005]. This can be a feature of a small storm, since the July 21–23, 2009 was a small storm with Dst more than −100 nT. In our previous modeling effort [*Ganushkina et al.*, 2010], two storms, one moderate with Dst about −120 nT and one intense with Dst about −250 nT, were modeled by the event-oriented magnetic field model [*Ganushkina et al.*, 2004] and the Space Weather Modeling Framework (SWMF) built around a global MHD simulation [*Toth et al.*, 2005]. It was found that the ring current showed a noticeable duskward shift for the intense storm but not for the moderate storm. It must be noted, however, that both storms were CME-driven. *Borovsky and Denton* [2010] have analyzed the magnetic field at geosynchronous orbit during High Speed Stream-driven storms. They found that the average value of the stretching and perturbations associated with the storm are greater in the midnight sector. They also pointed out that the stretching occurs in two phases: a strong stretching phase early in the storm followed by a modest stretching phase lasting for days. Since both ring current and near-Earth tail current contribute to the field line stretching at 6.6 R_E, the maximum of stretching on the nightside coincides with our results, to some extent. The question whether it is a feature of small storms or CIR-driven storms may be interesting to study.

[62] When contributions to the Dst index from different current systems are determined based on the magnetospheric magnetic field models, they are usually calculated using the representations of the current systems in the models. According to the TS05 model (Figure 6), the main contribution comes from the tail current module. The tail current dominance was present in modeling for other types of storms [*Tsyganenko and Sitnov*, 2005]. If we do not directly calculate the magnetic field from the model current systems but determine the regions of current lines which correspond to different current systems, we will obtain a very different

result (Figure 7). For quiet conditions, the location of the tail current given by the model current density of the tail current module was consistent with the area at X_{GSM} from -8 to -12 R_E occupied by the current lines which close at the magnetopause. For the storm main phase, the tail current density had two peaks, with the earthward peak coinciding with the area of current lines with both ends at the Earth's surface and going around the Earth. Thus, the peaks in the tail current density do not always correspond to the current lines having both ends at the magnetopause and are in the region, where current lines look more like ring current. Therefore, the tail current contribution presented in Figure 6 contains the contributions from other current systems than those which have both ends at the magnetopause. The analysis presented above stresses once more that the current lines are not identical to particle trajectories. Moreover, currents cannot be defined solemnly by the parameters of the local plasma populations. As was pointed out by *Liemohn et al.* [2011], magnetospheric currents should be defined by the current lines and their closures. It was shown that the same particle can contribute to several current systems when it moves.

[63] Figure 7 requires additional discussion. It may seem to be different from well-known pattern of symmetric and asymmetric (partial) ring currents. Figures 7b and 7c show that during the storm main phase there exist two regions of current lines going around the Earth, one earthward from -4 R_E and another at distances from -6 to -10 R_E with the region of current lines closed to the ionosphere between them. Similar configuration, where partial ring current can be inside of symmetric ring current was presented by *Liemohn et al.* [2011]. As it was already mentioned above, the ion drift is not equal to the total current flow. We obtained Figure 7 from the TS05 model with the numerical accuracy of current line tracing procedure tested on analytical models. For comparison, Figure 7a shows "traditional" distribution of the ring and tail currents for quiet conditions. When analyzing the Figure 7, it should be kept in mind that the TS05 model was created to reproduce the observed magnetic field. It was not tested on how accurate the models can reproduce real current density vectors. Another important thing is that the geometry of the TS05 ring current on the nightside is not consistent with the position of the inner edge of tail current module. This can lead to the configuration with the thin current sheet piercing the thick symmetric ring current on nightside.

[64] At the same time, the tail current is an important contributor to the Dst index. The division of the IMPTAM modeling region into three regions corresponding to eastward ring current, westward ring current and near-Earth part of the tail current (Figure 11) was very approximate. Relation between contributions from the tail and ring currents to the SymH index depends very much on the locations of regions where these currents flow. Moreover, during different phases of magnetic storms, boundaries between regions can change significantly and, therefore, the relative contributions to the SymH index. In the present study the important thing is that the current at about 6 to 10 R_E can contribute significantly to the total model Dst index. In our simulations we did not have any restrictions on the locations of the model boundary. Usually in the ring current models, the outer boundary is set at 6.6 R_E, where the plasma density and temperature observations are available from the LANL geostationary satellites [*Bame et al.*, 1993]. These measurements can then be used to determine the boundary conditions in the plasma sheet [*Jordanova et al.*, 2006; *Liemohn et al.*, 2001; *Ganushkina et al.*, 2006]. The particles inside geostationary orbit are identified as the ring current particles. As a result, the Dst minimum is significantly underestimated during storm-time ring current modeling [see, e.g., *Jordanova et al.*, 2006]. A time-dependent model boundary outside of 6.6 R_E gives a possibility to take into account the particles in the transition region (between dipole and stretched field lines, when nondipolar magnetic field is used) forming a partial ring current and near-Earth tail current in that region. *Ganushkina et al.* [2011] made a comparison between the calculations of the model SymH by Biot-Savart's law and by widely used Dessler-Parker-Sckopke (DPS) relation when modeling the ring current with IMPTAM for storm times and using nondipolar magnetic fields. Biot-Savart's Dst calculations resulted in larger and more realistic values. Using Biot-Savart's law, the modeled SymH* is not assumed to come from the ring current energy only. The effect from the near-Earth tail current is included by the presence of the stretched magnetic field lines.

7. Conclusions

[65] Keeping the points discussed above in mind, the conclusions are as follows:

[66] 1. For the CIR/HSS-driven storm on July 21–23, 2009, our attempts to modify the TS05 Tsyganenko model did not provide a better model than the standard TS05. The magnitudes of current densities in the inner magnetosphere computed with IMPTAM are comparable to those of computed with the TS05 magnetic field model. More than a factor of ten increase was seen in the ring and near-Earth currents during the storm main phase. The ring current, being asymmetric during the storm main phase and symmetrizing during the storm recovery phase, did not show a duskward shift of its peak during considered time interval.

[67] 2. It is very important to include the near-Earth tail currents in the calculations of model SymH or Dst indices. The incorporation of near-Earth tail currents in the calculations of model SymH or Dst indices is crucial, as there is significant current beyond 6.6 R_E in the simulation results.

[68] 3. The method to calculate the contributions of different current systems to the model Dst using the global magnetospheric magnetic field models should be Biot-Savart integration inside the regions, which contain the current systems, not using the magnetic field from the model representations of current modules. A discrepancy is found between the SymH contributions from various currents as defined by the TS05 modules and from current streamline tracing through these same currents. This is because of spatial overlap in the definitions of the current systems, yielding current streamlines that close around the Earth extending beyond the ring current region (and into the tail current region) as defined in the TS05 modules.

[69] **Acknowledgments.** We thank OMNIWEB data center for IMF and solar wind parameter data, World Data Center C2 for Geomagnetism, Kyoto, for the provisional *AE*, *Kp*, and *Dst* indices data. We thank Howard Singer at NOAA Space Weather Prediction Center for his preparation of GOES magnetometer data. We thank K.H. Glassmeier and H.U. Auster

for the use of THEMIS FGM data provided under the lead of the Technical University of Braunschweig. We acknowledge NASA contract NAS5-02099 and V. Angelopoulos for use of data from the THEMIS Mission. Specifically, C. W. Carlson and J. P. McFadden for use of ESA data, D. Larson and R. P. Lin for use of SST data. We thank D. Turner and P. Cruse for help with SST data processing. S. Dubyagin's work was fully supported and N. Ganushkina's work was partly supported by the Academy of Finland. N. Ganushkina gratefully acknowledges the support of part of this work by NASA and NSF grants. A. Runov acknowledges NSF for financial support through grant 1044495. The authors are very grateful to N. Tsyganenko for very helpful discussions and comments.

[70] Masaki Fujimoto thanks the reviewers for their assistance in evaluating this paper.

References

Alexeev, I. I., E. S. Belenkaya, V. V. Kalegaev, Y. I. Feldstein, and A. Grafe (1996), Magnetic storms and magnetotail currents, *J. Geophys. Res.*, *101*, 7737–7747.

Alexeev, I. I., V. V. Kalegaev, E. S. Belenkaya, S. Y. Bobrovnikov, Y. I. Feldstein, and L. I. Gromova (2001), Dynamic model of the magnetosphere: Case study for January 9–12, 1997, *J. Geophys. Res.*, *106*, 25,683–25,693.

Angelopoulos, V. (2008), The THEMIS mission, *Space Sci. Rev.*, *141*, 5–34, doi:10.1007/s11214-008-9336-1.

Auster, H. U., et al. (2008), The THEMIS Fluxgate Magnetometer, *Space Sci. Rev.*, *141*, 235–264.

Bame, S. J., D. J. McComas, M. F. Thomsen, B. L. Barraclough, R. C. Elphic, J. P. Glore, J. T. Gosling, J. C. Chavez, E. P. Evans, and F. J. Wymer (1993), Magnetospheric plasma analyzer for spacecraft with constrained resources, *Rev. Sci. Instr.*, *64*, 1026–1033.

Borovsky, J. E., and M. H. Denton (2006), Differences between CME-driven storms and CIR-driven storms, *J. Geophys. Res.*, *111*, A07S08, doi:10.1029/2005JA011447.

Borovsky, J. E., and M. H. Denton (2010), Magnetic field at geosynchronous orbit during high-speed stream-driven storms: Connections to the solar wind, the plasma sheet, and the outer electron radiation belt, *J. Geophys. Res.*, *115*, A08217, doi:10.1029/2009JA015116.

Boyle, C., P. Reiff, and M. Hairston (1997), Empirical polar cap potentials, *J. Geophys. Res.*, *102*, 111–125.

Burlaga, L. F., and R. P. Lepping (1977), The causes of recurrent geomagnetic storms, *Planet. Space Sci.*, *25*, 1151–1160.

Buzulukova, N. Y., Y. I. Galperin, R. A. Kovrazhkin, A. L. Glazunov, G. A. Vladimirova, H. Stenuit, J. A. Sauvaud, and D. C. Delcourt (2002), Two types of ion spectral gaps in the quiet inner magnetosphere: Interball-2 observations and modeling, *Ann. Geophys.*, *20*, 349–364.

Buzulukova, N. Y., R. A. Kovrazhkin, A. L. Glazunov, J.-A. Sauvaud, N. Y. Ganushkina, T. I. Pulkkinen (2003), Stationary nose structures of protons in the inner magnetosphere: Observations by the ION spectrometer onboard INTERBALL-2 satellite and modelling, *Cosmic Res.*, *41*, 3–12.

Carpenter, D., and R. Anderson (1992), An ISEE/whistler model of equatorial electron density in the magnetosphere, *J. Geophys. Res.*, *97*, 1097–1108.

Chen, M. W., M. Schulz, L. R. Lyons, and D. J. Gorney (1993), Stormtime transport of ring current and radiation belt ions, *J. Geophys. Res.*, *98*, 3835–3849.

Denton, M. H., J. E. Borovsky, R. M. Skoug, M. F. Thomsen, B. Lavraud, M. G. Henderson, R. L. McPherron, J. C. Zhang, and M. W. Liemohn (2006), Geomagnetic storms driven by ICME- and CIR-dominated solar wind, *J. Geophys. Res.*, *111*, A07S07, doi:10.1029/2005JA011436.

Dremukhina, L. A., Y. I. Feldstein, I. I. Alexeev, V. V. Kalegaev, and M. E. Greenspan (1999), Structure of the magnetospheric magnetic field during magnetic storms, *J. Geophys. Res.*, *104*, 28,351–28,360.

Ebihara, Y., and M. Ejiri (2000), Simulation study on fundamental properties of the storm-time ring current, *J. Geophys. Res.*, *105*, 15,843–15,859, doi:10.1029/1999JA900493.

Ebihara, Y., and M.-C. Fok (2004), Postmidnight storm-time enhancement of tens-of-keV proton flux, *J. Geophys. Res.*, *109*, A12209, doi:10.1029/2004JA010523.

Ejiri, M., R. A. Hoffman, and P. H. Smith (1980), Energetic particle penetrations into the inner magnetosphere, *J. Geophys. Res.*, *85*, 653–663.

Fok, M.-C., J. U. Kozyra, A. F. Nagy, C. E. Rasmussen, and G. V. Khazanov (1993), Decay of equatorial ring current ions and associated aeronomical consequences, *J. Geophys. Res.*, *98*, 19,381–19,393, doi:10.1029/93JA01848.

Fok, M.-C., et al. (2003), Global ENA image simulations, *Space Sci. Rev.*, *109*, 77–103, doi:10.1023/B:SPAC.0000007514.56380.fd.

Ganushkina, N. Y. (2011), IMPTAM: Including self-consistent magnetic field in ring current modeling, paper presented at Joint CEDAR-GEM Workshop, IUGG Gen. Assem., Santa Fe, N. M.

Ganushkina, N. Y., T. I. Pulkkinen, V. F. Bashkirov, D. N. Baker, and X. Li (2001), Formation of intense nose structures, *Geophys. Res. Lett.*, *28*, 491–494.

Ganushkina, N. Y., T. I. Pulkkinen, M. V. Kubyshkina, H. J. Singer, and C. T. Russell (2002), Modeling the ring current magnetic field during storms, *J. Geophys. Res.*, *107*(A7), 1092, doi: 10.1029/2001JA900101.

Ganushkina, N. Y., T. I. Pulkkinen, M. V. Kubyshkina, H. J. Singer, and C. T. Russell (2004), Long-term evolution of magnetospheric current systems during storms, *Ann. Geophys.*, *22*, 1317–1334.

Ganushkina, N. Y., T. I. Pulkkinen, T. Fritz (2005), Role of substorm-associated impulsive electric fields in the ring current development during storms, *Ann. Geophys.*, *23*, 579–591.

Ganushkina, N. Y., T. I. Pulkkinen, A. Milillo, and M. Liemohn (2006), Evolution of the proton ring current energy distribution during April 21–25, 2001 storm, *J. Geophys. Res.*, *111*, A11S08, doi:10.1029/2006JA011609.

Ganushkina, N. Y., M. Liemohn, M. Kubyshkina, R. Ilie, and H. Singer (2010), Distortions of the magnetic field by storm-time current systems in Earth's magnetosphere, *Ann. Geophys.*, *28*, 123–140.

Ganushkina, N. Y., M. W. Liemohn, and T. I. Pulkkinen (2011), Storm-time ring current: Model-dependent results, *Ann. Geophys.*, *30*, 177–202.

Gonzalez, W. D., B. T. Tsurutani, and A. L. Clua de Gonzalez (1999), Interplanetary origin of geomagnetic storms, *Space Sci. Rev.*, *88*, 529–562.

Gosling, J. T., D. J. McComas, J. L. Phillips, and S. J. Bame (1991), Geomagnetic activity associated with Earth passage of interplanetary shock disturbances and coronal mass ejections, *J. Geophys. Res.*, *96*, 7831–7839, doi:10.1029/91JA00316.

Hedin, A. (1991), Extension of the MSIS thermosphere model into the middle and lower atmosphere, *J. Geophys. Res.*, *96*, 1159–1172.

Hilmer, R. V., and G.-H. Voigt (1995), A magnetospheric magnetic field model with flexible current systems driven by independent physical parameters, *J. Geophys. Res.*, *100*, 5613–5626.

Janev, R. K., and J. J. Smith (1993), Cross sections for collision processes of hydrogen atoms with electrons, protons, and multiply-charged ions, in *Atomic and Plasma-Material Interaction Data for Fusion*, vol. 4, pp. 78–79, Int. At. Energ. Agency, Vienna.

Jordanova, V. K., L. M. Kistler, J. U. Kozyra, G. V. Khazanov, and A. F. Nagy (1996), Collisional losses of ring current ions, *J. Geophys. Res.*, *101*, 111–126, doi:10.1029/95JA02000.

Jordanova, V. K., Y. S. Miyoshi, S. Zaharia, M. F. Thomsen, G. D. Reeves, D. S. Evans, C. G. Mouikis, and J. F. Fennell (2006), Kinetic simulations of ring current evolution during the Geospace Environment Modeling challenge events, *J. Geophys. Res.*, *111*, A11S10, doi:10.1029/2006JA011644.

Jordanova, V. K., H. Matsui, P. A. Puhl-Quinn, M. F. Thomsen, K. Mursula, and L. Holappa (2009), Ring current development during high speed streams, *J. Atmos. Sol. Terr. Phys.*., *71*, 1093–1102.

Kalegaev, V. V., N. Y. Ganushkina, T. I. Pulkkinen, M. V. Kubyshkina, H. J. Singer, and C. T. Russell (2005), Relation between the ring current and the tail current during magnetic storms, *Ann. Geophys.*, *23*, 523–533.

Khazanov, G. V., M. W. Liemohn, M.-C. Fok, T. S. Newman, and A. J. Ridley (2004), Stormtime particle energization with AMIE potentials, *J. Geophys. Res.*, *109*, A05209, doi:10.1029/2003JA010186.

Kozyra, J. U., M. W. Liemohn, C. R. Clauer, A. J. Ridley, M. F. Thomsen, J. E. Borovsky, J. L. Roeder, V. K. Jordanova, and W. D. Gonzalez (2002), Multistep Dst development and ring current composition changes during the 4–6 June 1991 magnetic storm, *J. Geophys. Res.*, *107*(A8), 1224, doi:10.1029/2001JA000023.

Kubyshkina, M. V., V. A. Sergeev, and T. I. Pulkkinen (1999), Hybrid Input Algorithm: An event-oriented magnetospheric model, *J. Geophys. Res.*, *104*, 24,977–24,993, doi:10.1029/1999JA900222.

Kubyshkina, M. V., T. I. Pulkkinen, N. Y. Ganushkina, and N. Partamies (2008), Magnetospheric currents during sawtooth events: Event-oriented magnetic field model analysis, *J. Geophys. Res.*, *113*, A08211, doi:10.1029/2007JA012983.

Kubyshkina, M. V., V. Sergeev, N. Tsyganenko, V. Angelopoulos, A. Runov, H. Singer, K. H. Glassmeier, H. U. Auster, and W. Baumjohann (2009), Toward adapted time-dependent magnetospheric models: A simple approach based on tuning the standard model, *J. Geophys. Res.*, *114*, A00C21, doi:10.1029/2008JA013547.

Le, G., C. T. Russell, and K. Takahashi (2004), Morphology of the ring current derived from magnetic field observations, *Ann. Geophys.*, *22*, 1267–1295.

Lemon, C., F. Toffoletto, M. Hesse, and J. Birn (2003), Computing magnetospheric force equilibria, *J. Geophys. Res.*, *108*(A6), 1237, doi:10.1029/2002JA009702.

Liemohn, M. W., J. U. Kozyra, M. F. Thomsen, J. L. Roeder, G. Lu, J. E. Borovsky, and T. E. Cayton (2001), Dominant role of the asymmetric ring current in producing the stormtime *Dst**, *J. Geophys. Res.*, *106*, 10,883–10,904.

Liemohn, M. W., A. J. Ridley, P. C. Brandt, D. L. Gallagher, J. U. Kozyra, D. M. Ober, D. G. Mitchell, E. C. Roelof, and R. DeMajistre (2005), Parametric analysis of nightside conductance effects on inner magnetospheric dynamics for the 17 April 2002 storm, *J. Geophys. Res.*, *110*, A12S22, doi:10.1029/2005JA011109.

Liemohn, M. W., A. J. Ridley, J. U. Kozyra, D. L. Gallagher, M. F. Thomsen, M. G. Henderson, M. H. Denton, P. C. Brandt, and J. Goldstein (2006), Analyzing electric field morphology through data-model comparisons of the GEM IM/S Assessment Challenge events, *J. Geophys. Res.*, *111*, A11S11, doi: 10.1029/2006JA011700.

Liemohn, M. W., D. L. De Zeeuw, R. Ilie, and N. Y. Ganushkina (2011), Deciphering magnetospheric cross-field currents, *Geophys. Res. Lett.*, *38*, L20106, doi:10.1029/2011GL049611.

Lui, A. T. Y. (2003), Inner magnetospheric plasma pressure distribution and its local time asymmetry, *Geophys. Res. Lett.*, *30*(16), 1846, doi:10.1029/2003GL017596.

Lui, A. T. Y., R. W. McEntire, and S. M. Krimigis (1987), Evolution of the ring current during two geomagnetic storms, *J. Geophys. Res.*, *92*, 7459–7470.

Lui, A. T. Y., H. E. Spence, and D. P. Stern (1994), Empirical modeling of the quiet time nightside magnetosphere, *J. Geophys. Res.*, *99*, 151–157.

McFadden, J. P., C. W. Carlson, D. Larson, M. Ludlam, R. Abiad, B. Elliott, P. Turin, M. Marckwordt, and V. Angelopoulos (2008), The THEMIS ESA plasma instrument and in-flight calibration, *Space Sci. Rev.*, *141*, 277–302, doi:10.1007/s11214–008–9440–2.

Miyoshi, Y., and R. Kataoka (2008), Flux enhancement of the outer radiation belt electrons after the arrival of stream interaction regions, *J. Geophys. Res.*, *113*, A03S09, doi:10.1029/2007JA012506.

Ohtani, S., M. Nosé, G. Rostoker, H. Singer, A. T. Y. Lui, and M. Nakamura (2001), Storm substorm relationship: Contribution of the tail current to Dst, *J. Geophys. Res.*, *106*, 21,199–21,209.

Ohtani, S., P. C. Brandt, H. J. Singer, D. G. Mitchell, and E. C. Roelof (2006), Statistical characteristics of hydrogen and oxygen ENA emission from the storm-time ring current, *J. Geophys. Res.*, *111*, A06209, doi:10.1029/2005JA011201.

Ohtani, S., Y. Ebihara, and H. J. Singer (2007), Storm-time magnetic configurations at geosynchronous orbit: Comparison between the main and recovery phases, *J. Geophys. Res.*, *112*, A05202, doi:10.1029/2006JA011959.

Parker, E. N., and H. A. Stewart (1967), Nonlinear inflation of a magnetic dipole, *J. Geophys. Res.*, *72*, 5287–5293.

Pulkkinen, T. I., N. Y. Ganushkina, E. I. Tanskanen, M. V. Kubyshkina, G. D. Reeves, M. F. Thomsen, C. T. Russell, H. J. Singer, J. A. Slavin, and J. Gjerloev (2006), Magnetospheric current systems during storm-time sawtooth events, *J. Geophys. Res.*, *111*, A11S17, doi: 10.1029/2006JA011627.

Richardson, I. G., et al. (2006), Major geomagnetic storms (Dst ≥ −100 nT) generated by corotating interaction regions, *J. Geophys. Res.*, *111*, A07S09, doi:10.1029/2005JA011476.

Roederer, J. G. (1970), *Dynamics of Geomagnetically Trapped Radiation*, 36 pp., Springer, New York.

Roelof, E. C., P. C. Brandt, and D. G. Mitchell (2004), Derivation of currents and diamagnetic effects from global plasma pressure distributions obtained by IMAGE/HENA, *Adv. Space Res.*, *33*, 747–751.

Sauvaud, J.-A., H. Barthe, C. Aoustin, J. Thocaven, J. Rouzaud, E. Penou, D. Popescu, R. Kovrazhkin, and K. Afanasiev (1998), The ION experiment onboard the Interball-Auroral satellite; initial results on velocity-dispersed structures in the cleft and inside the auroral oval, *Ann. Geophys.*, *16*, 1056–1069.

Shirai, H., K. Maezawa, M. Fujimoto, T. Mukai, Y. Saito, and N. Kaya (1997), Monoenergetic ion drop-off in the inner magnetosphere, *J. Geophys. Res.*, *102*, 19,873–19,881.

Sitnov, M. I., N. A. Tsyganenko, A. Y. Ukhorskiy, B. J. Anderson, H. Korth, A. T. Y. Lui, and P. C. Brandt (2010), Empirical modeling of a CIR-driven magnetic storm, *J. Geophys. Res.*, *115*, A07231, doi:10.1029/2009JA015169.

Smith, P. H., and R. A. Hoffman (1974), Direct observations in the dusk hours of the characteristics of the storm time ring current particles during the beginning of magnetic storms, *J. Geophys. Res.*, *79*, 966–971.

Søraas, F., K. Aarsnes, K. Oksavik, and D. S. Evans (2002), Ring current intensity estimated from low-altitude proton observations, *J. Geophys. Res.*, *107*(A7), 1149, 10.1029/2001JA000123.

Søraas, F., K. Aarsnes, K. Oksavik, M. I. Sandanger, D. S. Evans, and M. S. Greer (2004), Evidence for particle injection as the cause of Dst reduction during HILDCAA events, *J. Atmos. Sol. Terr. Phys.*, *66*, 177–186.

Sørbø, M., F. Søraas, M. I. Sandanger, and D. S. Evans (2009), Ring current behaviour during corotating interaction region and high speed stream events, *J. Atmos. Sol. Terr. Phys.*, *71*, 1103–1125.

Spiro, R. W., M. Harel, R. A. Wolf, and P. H. Reiff (1981), Quantitative simulation of a magnetospheric substorm: 3. Plasmaspheric electric fields and evolution of the plasmapause, *J. Geophys. Res.*, *86*, 2261–2272, doi:10.1029/JA086iA04p02261.

Stern, D. (1975), The motion of a proton in the equatorial magnetosphere, *J. Geophys. Res.*, *80*, 595–599.

Toffoletto, F., S. Sazykin, R. Spiro, and R. Wolf (2003), Inner magnetospheric modeling with the Rice Convection Model, *Space Sci. Rev.*, *107*, 175–196.

Toth, G., et al. (2005), Space Weather Modeling Framework: A new tool for the space science community, *J. Geophys. Res.*, *110*, A12226, doi:10.1029/2005JA011126.

Tsurutani, B. T., and W. D. Gonzalez (1997), The interplanetary causes of magnetic storms: A review, in *Magnetic Storms*, *Geophys. Monogr. Ser.*, vol. 98, edited by B. T. Tsurutani et al., pp. 77–89, AGU, Washington, D. C.

Tsurutani, B. T., et al. (2006), Corotating solar wind streams and recurrent geomagnetic activity: A review, *J. Geophys. Res.*, *111*, A07S01, doi:10.1029/2005JA011273.

Tsyganenko, N. A. (1989), A magnetospheric magnetic field model with a warped tail current sheet, *Planet. Space Sci.*, *37*, 5–20.

Tsyganenko, N. A. (1995), Modeling the Earth's magnetospheric magnetic field confined within a realistic magnetopause, *J. Geophys. Res.*, *100*, 5599–5612.

Tsyganenko, N. A. (2002a), A model of the near magnetosphere with a dawn-dusk asymmetry: 1. Mathematical structure, *J. Geophys. Res.*, *107*(A8), 1179, doi:10.1029/2001JA000219.

Tsyganenko, N. A. (2002b), A model of the near magnetosphere with a dawn-dusk asymmetry: 2. Parameterization and fitting to observations, *J. Geophys. Res.*, *107*(A8), 1176, doi: 10.1029/2001JA000220.

Tsyganenko, N. A., and T. Mukai (2003), Tail plasma sheet models derived from Geotail particle data, *J. Geophys. Res.*, *108*(A3), 1136, doi:10.1029/2002JA009707.

Tsyganenko, N. A., and M. I. Sitnov (2005), Modeling the dynamics of the inner magnetosphere during strong geomagnetic storms, *J. Geophys. Res.*, *110*, A03208, doi: 10.1029/2004JA010798.

Tsyganenko, N. A., and M. I. Sitnov (2007), Magnetospheric configurations from a high-resolution data-based magnetic field model, *J. Geophys. Res.*, *112*, A06225, doi:10.1029/2007JA012260.

Tsyganenko, N. A., H. J. Singer, and J. C. Kasper (2003), Storm-time distortion of the inner magnetosphere: How severe can it get?, *J. Geophys. Res.*, *108*(A5), 1209, doi: 10.1029/2002JA009808.

Turner, N. E., D. N. Baker, T. I. Pulkkinen, and R. L. McPherron (2000), Evaluation of the tail current contribution to Dst, *J. Geophys. Res.*, *105*, 5431–5439.

Vallat, C., I. Dandouras, M. Dunlop, A. Balogh, E. Lucek, G. K. Parks, M. Wilber, E. C. Roelof, G. Chanteur, and H. Rème (2005), First current density measurements in the ring current region using simultaneous multi-spacecraft CLUSTER-FGM data, *Ann. Geophys.*, *23*, 1849–1865.

Volland, H. (1973), A semiempirical model of large-scale magnetospheric electric fields, *J. Geophys. Res.*, *78*, 171–180.

Wolf, R. A., M. Harel, R. W. Spiro, G.-H. Voigt, P. H. Reiff, and C.-K. Chen (1982), Computer simulation of inner magnetospheric dynamics for the magnetic storm of July 29, 1977, *J. Geophys. Res.*, *87*, 5949–5962, doi:10.1029/JA087iA08p05949.

Zanetti, L. J., W. Baumjohann, T. A. Potemra, and P. F. Bythrow (1984), Three-dimensional Birkeland ionospheric current system, determined from Magsat, in *Magnetospheric Currents*, *Geophys.Monogr. Ser.*, vol. 28, edited by T. A. Potemra, pp. 123–130, AGU, Washington, D. C.

Zheng, Y., A. T. Y. Lui, M.-C. Fok, B. J. Anderson, P. C. Brandt, T. J. Immel, and D. G. Mitchell (2006), Relationship between Region 2 field-aligned current and the ring current: Model results, *J. Geophys. Res.*, *111*, A11S06, doi: 10.1029/2006JA011603.

S. Dubyagin, Finnish Meteorological Institute, PO Box 503, Helsinki FI-00101, Finland.

N. Y. Ganushkina and M. Liemohn, Department of Atmospheric, Oceanic, and Space Sciences, University of Michigan, 2455 Hayward St., Ann Arbor, MI 48109-2143, USA. (ganuna@umich.edu)

M. Kubyshkina, Institute of Physics, St. Petersburg State University, Ulyanovskaya 1, St. Petersburg 198504, Russia.

A. Runov, Institute of Geophysics and Planetary Physics, University of California, 3845 Slichter Hall, Los Angeles, CA 90095, USA.